Pu.1/Spi1 dosage controls the turnover and maintenance of microglia in zebrafish and mammals

Yi Wu[1#], Weilin Guo[2#], Haoyue Kuang[3], Xiaohai Wu[3], Thi Huong Trinh[2], Yuexin Wang[3], Shizheng Zhao[1], Zilong Wen[2,3], Tao Yu[1,3*]

[1]Biomedical Research Institute, Shenzhen Peking University-the Hong Kong University of Science and Technology Medical Center, Shenzhen 518036, China;

[2]Division of Life Science, the Hong Kong University of Science and Technology, Clear Water Bay, Hong Kong, China;

[3]Greater Bay Biomedical Innocenter, Shenzhen Bay Laboratory, Shenzhen 518055, China;

[#]These authors contribute equally to this work.

[*] Correspondence should be addressed to: tyu@connect.ust.hk

Abstract

Microglia are brain-resident macrophages playing pivotal roles in CNS development and homeostasis. Yet, the cellular and molecular basis governing microglia maintenance remains largely unknown. Here, via utilizing a visible conditional knockout allele of *pu.1* gene (the master regulator for microglia/macrophage lineage development) to generate mosaic microglia populations in adult zebrafish, we show that while *pu.1*-deficient microglia are immediate viable, they are less competitive and chronically eliminated through Tp53-mediated cell competition. Interestingly, when conditionally inactivating Pu.1 in adult *spi-b* (the orthologue of mouse *Spi-b*) null mutants, microglia are rapidly depleted via apoptosis, suggesting that Pu.1 and Spi-b regulate microglia maintenance in a dosage-dependent manner. The dosage-dependent regulation of microglia maintenance by PU.1 is evolutionarily conserved in mice, as shown by conditionally inactivating single and both *Pu.1* alleles in microglia respectively. Collectively, our study reveals the conserved cellular and molecular mechanisms controlling microglia turnover and maintenance in teleost and mammals.

Introduction

Microglia, the crucial immune cells residing in the central nervous system (CNS), have a profound impact on the maintenance of CNS homeostasis, as they not only function as scavengers to facilitate the removal of invading pathogens or damaged tissues, but also actively regulate neurogenesis, synaptic pruning and neuronal activity (Colonna & Butovsky, 2017, Gomez-Nicola & Perry, 2015).

It is therefore not surprising that the dysfunction of microglia is closely linked with the occurrence and progression of many neurodegenerative disorders (Glass, Saijo et al., 2010, Li, Du et al., 2012, Prinz, Priller et al., 2011), thus making it a promising therapeutic target in the prevention and treatment of these diseases.

In mice, fate-mapping methods revealed that unlike other glia cells with neuroectoderm origin, microglia in adult originate from yolk-sac (YS) derived primitive macrophages, which colonize the developing brain rudiment during early embryogenesis (Ginhoux, Greter et al., 2010, Schulz, Gomez Perdiguero et al., 2012). Whether microglia in adult mammals were contributed by monocyte-derived microglia precursors had long been a debate until the establishment of parabiosis assay (Ajami, Bennett et al., 2007). It is now well-accepted that under physiological condition microglia in mice are maintained locally by self-renewal throughout the lifespan. In accordance with this concept, microglia population was found to be rapidly reconstituted by resident cells after genetic or pharmacological ablation of microglia (Bruttger, Karram et al., 2015, Elmore, Najafi et al., 2014). However, when estimating the physiological turnover rate of microglia via different methods such as ^{3}H-thymidine/BrdU/EdU incorporation, Ki67 staining or two photon live imaging, different studies yielded distinct or even contradictory results i.e., the estimated microglia turnover rate ranging from 0.13 to 0.8% (Askew, Li et al., 2017, Füger, Hefendehl et al., 2017, Lawson, Perry et al., 1992, Tay, Mai et al., 2017), which indicated that microglia in adult mice (~2 years lifespan) were either long-lived without replenishment or replenished for several times during the whole lifespan of the animals. Nonetheless, these studies have reached the consensus that in adult mice all microglia have the proliferation capability and there are no putative microglia precursors existing to proliferate asymmetrically and continuously to contribute to microglia pool. Moreover, microglia proliferation had been shown to be spatially and temporally coupled with apoptosis to maintain the homeostasis of their population (Askew et al., 2017): which indicates that not only proliferating microglia locate near the dying microglia, but also newborn microglia manifest a higher frequency of apoptosis. However, whether this phenomenon is for the quality control of microglia or has any other physiological relevance remained unclear. In addition, as a fraction of newborn microglia underwent apoptosis and did not contribute to microglia homeostasis, previously calculated proliferation rate might potentially over-estimate the true turnover rate of microglia. Collectively, although these studies give some insights into the understanding of microglia turnover and maintenance, our knowledge about the underlying cellular and molecular mechanisms are still limited.

PU.1/SPI1, the founding member of the spleen focus forming virus proviral integration oncogene (SPI) subfamily of the E-twenty six (ETS) family transcription factor, is one of the best-characterized gene governing the development of macrophage lineage (McKercher, Torbett et al.,

1996, Scott, Simon et al., 1994). Disruption of PU.1 in mice causes early lethality of the embryos and complete absence of macrophages (McKercher et al., 1996, Scott et al., 1994), including microglia in brain (Kierdorf, Erny et al., 2013). Interestingly, the *PU.1* expression level was found to remain at a high level in microglia after their terminal differentiation (Walton, Gibbons et al., 2000), implying that PU.1 also regulates the cellular behaviors and functions of microglia in the sophisticated CNS environment. Indeed, Chromatin immunoprecipitation (ChIP)-Seq analysis with microglia cell line BV2 cells revealed thousands of PU.1 targets (Satoh, Asahina et al., 2014). Accordingly, silencing of PU.1 by siRNA in mixed human glial culture led to the reduced viability of microglia and decreased phagocytosis of amyloid-beta (Aβ42) (Smith, Gibbons et al., 2013). However, as a previous study reported that inactivating either 1 copy or 2 copies of PU.1 by fusing PU.1 with cytoplasm-retaining estrogen receptor (ER) had no effect on the viability of alveolar macrophages (Karpurapu, Wang et al., 2011), whether PU.1 indeed regulated the survival and maintenance of microglia in the in-vivo conditions remained to be further investigated. Moreover, human SNPs that altered *PU.1* expression level were reported to be associated with Alzheimer's disease (AD) pathogenesis (Cao, Zhou et al., 2022, Huang, Marcora et al., 2017). A recent study showed that conditional inactivation or pharmacological inhibition of PU.1 in AD mouse model ameliorated neuroinflammation, prevented microgliosis and improved cognitive performance (Ralvenius, Mungenast et al., 2023). Although reduction of microglia number was considered as a result of the amelioration of neuroinflammation, whether PU.1 directly regulated microglia survival and maintenance to prevent the propagation of neuroinflammation in diseased condition deserved to be carefully revisited. SPI-B, another member in the mammalian SPI subfamily, has been shown to be dispensable for the development of the macrophage lineage (Su, Chen et al., 1997). Yet, its involvement in the regulation of microglia turnover and maintenance remains to be investigated.

Owing to the genetic amenability and the feasibility for live-imaging and lineage tracing, zebrafish has been adopted as an ideal model for the study of microglia development and function (Hughes & Appel, 2020, Iyer, Shen et al., 2022, Li et al., 2012, Peri & Nüsslein-Volhard, 2008). Zebrafish microglia are highly conserved with their mammalian counterparts in terms of morphology, molecular signatures, development-regulatory genetic networks as well as functions (Xu, Zhu et al., 2015, Yu, Guo et al., 2017). Different from the single origin of mouse microglia, zebrafish microglia were shown to arise from two distinct sources i.e., the rostral blood island (RBI), equivalent of mouse YS for primitive myelopoiesis, and the aorta-gonad-mesonephros (AGM) region for hematopoietic stem cell (HSC) initiation. The RBI microglia colonize the developing brain during early embryogenesis, but are gradually replenished by AGM adult microglia (Xu et al., 2015). Further study revealed that this dynamic shift of microglia pool is controlled by Il34-Csf1ra signaling-dictated cell competition (Yu, Kuang et al., 2023). Yet, when

the microglia pool is established in adult zebrafish, the molecular mechanisms underlying their turnover and maintenance remain incompletely understood. Moreover, although Pu.1 (also called Spi1b, Ensembl:ENSDARG00000000767) and its paralogue Spi-b (also called Spi1a, Ensembl:ENSDARG00000067797), the zebrafish orthologues of mammalian PU.1 and SPI-B, were shown to be indispensable for microglia early development of both origins in zebrafish (Xu et al., 2015, Yu et al., 2017), their functions in the survival and maintenance of microglia in adult animals have not been established.

In the present study, via the condition knockout strategy to generate mosaic microglia population in adult zebrafish and mice, we revealed that the turnover and maintenance of microglia is evolutionarily conserved and regulated by Pu.1/Spi1 dosage from teleost to mammals.

Results

Adult microglia in zebrafish undergo rapid turnover and random proliferation to replenish and maintain their pool

Previous studies have shown that there are two major subtypes of myeloid cells, i.e., *ccl34b.1*$^{+}$ microglia and *ccl34b.1*$^{-}$*ccl19a.1*$^{+}$ brain-resident dendritic cells (DCs) in adult zebrafish brain (Wu, Nguyen et al., 2020, Zhou, Zhao et al., 2023). To monitor the turnover and maintenance of microglia in adult zebrafish brain, we employed microglia-specific *TgBAC(ccl34b.1:eGFP)* transgenic reporter line (Wu et al., 2020) and performed EdU pulse-chase experiment, a similar strategy with that in mouse to determine microglia turnover (Askew et al., 2017, Tay et al., 2017). As a single dose of EdU injection might under-estimate the microglia turnover rate, we intraperitoneally injected EdU into adult *TgBAC(ccl34b.1:eGFP)* fish for either 1, 3 or 5 consecutive days. We then collected the fish brain at 1 day post injection (dpi) for cryosection and co-staining of eGFP, Lcp1 (a pan leukocyte marker expressed in both microglia and DCs), EdU and DAPI, in which ccl34b.1-eGFP^{+}Lcp1^{+} cells are microglia and ccl34b.1-eGFP^{-}Lcp1^{+} cells represent DCs (Fig. 1A). Quantification results showed that, while a single dose of EdU pulse labeled 1.892±0.234% microglia, the EdU incorporation rate for microglia after 3 or 5 doses of EdU pulses increased almost linearly (Fig. 1B, green bars). Based on these data, the estimated microglia turnover rate (daily) is ~2.6% (total EdU incorporation rate divided by the times of EdU-pulses) (Fig. 1C, green bars). On the other hand, the EdU incorporation rate for the DCs was much lower (Fig. 1B-C, red bars), suggesting that the DCs in the brain are relatively steady with a very low turnover rate.

Previously, via the EdU/BrdU dual-pulse assay, Tay et al. have shown that microglia in adult mouse brain proliferate randomly during homeostasis and no putative microglia precursors have

been identified accordingly (Tay et al., 2017). To clarify whether there might be putative microglial precursors that continuously proliferate to contribute to microglia turnover in zebrafish, we employed a similar strategy, in which adult wild-type (WT) fish were injected with a single dose of EdU followed with five daily BrdU pulses to determine the BrdU proliferation rate of EdU^+ and EdU^- microglia (Fig. 1D, upper panel). Quantification result showed that the BrdU incorporation rates were comparable between EdU^+ and EdU^- microglia pools (Fig. 1D-E). These data strongly suggest that, similar to mammals (Tay et al., 2017), microglia in adult zebrafish randomly undergo proliferation and there are no well-defined microglial precursors that continuously proliferate to replenish and maintain the microglia pool.

Generation and characterization of the visible conditional knockout allele *pu.1^{KI}*

To elucidate the molecular mechanisms underlying microglia turnover and maintenance, we focused on the Ets family transcription factor PU.1/SPI1, which had been shown to be a master regulator for macrophage/microglia development in fish and mammals (McKercher et al., 1996, Scott et al., 1994, Yu et al., 2017). Because macrophages/microglia development is completely blocked at early development in *pu.1*-null zebrafish mutants (Yu et al., 2017), we decided to generate a visible *pu.1* conditional knockout allele *pu.1^{KI}* to study the role of Pu.1 in microglia maintenance via the Non-homologous end joining (NHEJ)-mediated knock-in method (Fig. 2A and Fig. S1A) (Li, Zhang et al., 2015). As shown in Fig. 2A, the knock-in DNA fragment consisted of loxP, *pu.1* exon 4 to 6 followed by the self-cleaving P2A sequence-conjugated eGFP, and a splicing-acceptor site SpA2 followed by the P2A-DsRed. In addition, the 3' downstream sequence of *pu.1* gene (gray box) was added to the 3' end of each fluorescent protein to ensure efficient termination of RNA transcription and proper expression of the fluorescent proteins.

Three different founders were obtained. PCR and deep sequencing analysis of F1 embryos confirmed the correct integration of donor DNA fragment in the *pu.1* locus (Fig. S1B-C). Since the knock-in *pu.1^{KI}* allele would generate intact Pu.1 and eGFP concurrently (Fig. 2A), we predicted the expression pattern of eGFP, which presumably represents the expression of the knock-in Pu.1, should completely overlap with the endogenous Pu.1. Indeed, co-staining of eGFP and Pu.1 antibodies revealed a perfect overlap of the $eGFP^+$ cells and $Pu.1^+$ cells in *pu.1$^{KI/+}$* embryos (Fig. 2B), suggesting that the *pu.1^{KI}* allele recapitulates the expression of endogenous *pu.1*. Further studies suggested that *pu.1^{KI}-eGFP* efficiently labels embryonic microglia, and both microglia and DCs in adult, as revealed by the co-localization of *pu.1^{KI}-eGFP* and macrophage-specific reporter line *Tg(mpeg1:LRLG)* at 3 dpf, and by the co-staining of eGFP and Lcp1 antibodies on the brain sections of adult *pu.1$^{KI/+}$* fish respectively (Fig. 2C and D). To further confirm functional intactness of the *pu.1^{KI}* allele, we crossed the *pu.1^{KI}* fish with the *pu.1$^{\Delta 839}$* mutants to examine if the *pu.1^{KI}*

allele is capable of rescuing the microglia phenotype. Indeed, quantification of microglia number revealed no difference between the *pu.1*$^{\Delta 839/KI}$ and *pu.1*$^{\Delta 839/+}$ embryos (Fig. 2E and F), indicating that the *pu.1*^{KI} allele functionally recapitulates the endogenous *pu.1*.

To test whether the Cre mediated excision occurs correctly in the *pu.1*^{KI} allele, we injected Cre mRNA into the *pu.1*^{KI} embryos at one-cell stage. The injected embryos were raised to adulthood (*pu.1*^{CKO} fish) and crossed with the *pu.1*^{KI} fish to generate *pu.1*$^{CKO/KI}$ fish. As illustrated in Fig. 2A, the Cre-mediated excision should remove the E4-6-P2A-eGFP cassette and allow the proper splicing of the splicing-acceptor site SpA2 and joining of the P2A-DsRed with exon 3 (Fig. 2A), leading to the induction of DsRed expression. Indeed, fluorescent imaging of the *pu.1*$^{CKO/KI}$ embryos revealed robust DsRed (*pu.1*^{CKO} allele) signals perfectly overlapping with the eGFP (*pu.1*^{KI} allele) signals (Fig 2G), suggesting the correct DNA excision and RNA splicing in the *pu.1*^{CKO} allele. This conclusion was further validated by sequencing analysis of the *pu.1*^{CKO} transcripts (Fig. 2H). Since the endogenous *pu.1* exons were not replaced, but instead they were separated far away from the upstream exons by donor plasmid, we performed quantitative RT-PCR analysis of *pu.1*$^{CKO/CKO}$ embryos to determine the possible expression of the endogenous *pu.1* exons in *pu.1*^{CKO} allele. The result showed that the relative expression of endogenous *pu.1* exons is around 1~2% in comparison with that of DsRed expression (Fig. S1D), suggesting that expression of *pu.1* is largely abolished in *pu.1*^{CKO} allele. To phenotypically characterize *pu.1*^{CKO} allele, and to avoid incomplete inactivation of Pu.1 function in downstream microglia tracing experiments, which may occur when using two *pu.1*^{KI} alleles due to the lower CreER recombination efficiency in zebrafish compared to mice, we outcrossed the *pu.1*^{CKO} fish with the *pu.1*$^{\Delta 839}$ null mutants. As anticipated, the development of embryonic microglia was completely blocked in the *pu.1*$^{CKO/\Delta 839}$ embryos (Fig. 2I and J), a phenotype recapitulating the defect of the *pu.1*$^{\Delta 839}$ homozygous mutants (Yu et al., 2017). These data demonstrate that the *pu.1*^{KI} allele works very well and serves as a useful tool to explore the role of Pu.1 in adult microglia survival and maintenance.

Pu.1 and Spi-b regulate the turnover and maintenance of microglia in a dosage-dependent manner

To investigate the role of Pu.1 in the survival and maintenance of microglia in adult zebrafish, we crossed the *pu.1*^{KI} fish with the leukocyte-specific *Tg(coro1a:CreER)* line and the *pu.1*$^{\Delta 839}$ mutants to generate *pu.1*$^{KI/+}$*;Tg(coro1a:CreER)* and *pu.1*$^{KI/\Delta 839}$*;Tg(coro1a:CreER)* fish. We then intraperitoneally injected 3 doses of 4-OHT into these adult fish and collected the brain samples at 2 dpi and 8 dpi for the quantification of microglia number after cryo-section and eGFP/DsRed immuno-staining (Fig. 3A, upper panel). As shown in Fig. 3A (lower panel), DsRed^{+} cells were readily detected in the brains of both *pu.1*$^{KI/+}$*;Tg(coro1a:CreER)* and *pu.1*$^{KI/\Delta 839}$*;Tg(coro1a:CreER)*

fish at 8 dpi. Quantification of the number and proportion of DsRed^{+} cells at 2 dpi and 8 dpi revealed no difference between *pu.1*$^{KI/\Delta 839}$*;Tg(coro1a:CreER)* mutant fish and *pu.1*$^{KI/+}$*;Tg(coro1a:CreER)* control siblings (Fig. 3B-C). Similarly, conditional knockout of *pu.1* in embryonic microglia also showed no effect on microglial survival (Figure S2), which contrasts to the elimination of microglia during early development by global knockout of *pu.1* due to Pu.1's essential role in myeloid lineage specification. In addition, we also found that the number and proportion of microglia (ccl34b.1-eGFP^{+} Lcp1^{+}) and DCs (ccl34b.1-eGFP^{-}Lcp1^{+}) were comparable between *pu.1*$^{\Delta 839/\Delta 839}$*;TgBAC(ccl34b.1:eGFP)* null mutants and *pu.1*$^{\Delta 839/+}$*;TgBAC(ccl34b.1:eGFP)* siblings (Fig. S3). These data suggest that Pu.1 is not required for the survival of microglia and DCs. We reasoned that the survival of *pu.1*-deficient microglia is likely attributed to the presence of *spi-b* (the paralogue of *pu.1* in zebrafish, also called *spi1a*), which has been shown to play a compensatory role for Pu.1 in microglia early development (Yu et al., 2017). Indeed, conditional inactivation of Pu.1 in the *spi-b*$^{\Delta 232/\Delta 232}$ null mutants led to a rapid depletion of microglia by apoptosis within several days (Fig. S4 and Fig. S5), indicating that Pu.1 and Spi-b act redundantly to regulate the survival of microglia.

To further investigate whether Pu.1-deficiency might have a long-term effect on the turnover and maintenance of microglia, we traced *pu.1*-deficient DsRed^{+} cells to 1 month post injection (mpi), and 3 mpi after conditionally inactivating Pu.1 in adult *pu.1*$^{KI/+}$*;Tg(coro1a:CreER)* and *pu.1*$^{KI/\Delta 839}$*;Tg(coro1a:CreER)* fish (Fig. 3D, upper panel). Intriguingly, we found that the number and proportion of DsRed^{+} cells in the midbrains of the *pu.1*$^{KI/\Delta 839}$*;Tg(coro1a:CreER)* fish began to decline at 1 mpi and were further reduced, becoming significantly lower than that in *pu.1*$^{KI/+}$*;Tg(coro1a:CreER)* fish by 3 mpi (Fig.3E-F). Likewise, the number and proportion of DsRed^{+} cells in the retina and spinal cord were also significantly reduced in the *pu.1*$^{KI/\Delta 839}$*;Tg(coro1a:CreER)* fish by 3 mpi (Fig. S6). Since microglia are the major population of the *coro1a*$^{+}$ cells in the brain and spinal cord and the exclusive population in the retina (Wu et al., 2020), the reduction of DsRed^{+} cells in the *pu.1*$^{KI/\Delta 839}$*;Tg(coro1a:CreER)* fish at 1 mpi and 3 mpi are mainly attributed to the loss of microglia. Based on the amoeboid and ramified morphology, microglia and DCs could be distinguished with about 90% accuracy (Fig. S7A-B). Thus, to further confirm above conclusion, we quantified microglia and DCs separately in 3-mpi *pu.1*$^{KI/+}$*;Tg(coro1a:CreER)* and *pu.1*$^{KI/\Delta 839}$*;Tg(coro1a:CreER)* fish. As anticipated, *pu.1*-deficient microglia were significantly reduced at 3 mpi (Fig. S7C-D). These results suggest that, although *pu.1* is dispensable for the immediate survival of microglia (Fig. 3B-C), it is essential for the turnover and long-term maintenance of microglia in adult zebrafish, which could not be fully compensated by *spi-b*.

_pu.1_-deficient microglia in mosaic condition were eliminated by cell competition

Given the fact that *pu.1*-deficient microglia are gradually eliminated in mosaic condition (Fig. 3E-F), but their number remains relatively normal in *pu.1*$^{\Delta 839}$ null mutants (Yu et al., 2017), we reasoned that the elimination of the *pu.1*-deficient microglia in mosaic condition is likely attributed to the cell competition between *pu.1*-deficient DsRed^{+} microglia and their neighboring eGFP^{+} sibling cells harboring WT *pu.1*. To test this hypothesis, we compared the cell death and proliferation rates of microglia by TUNEL and BrdU incorporation assays in both conditions respectively. To determine the cell death and proliferation rates of *pu.1*-deficient microglia in mosaic condition, we treated the adult *pu.1*$^{KI/\Delta 839}$*;Tg(coro1a:CreER)* fish with 4-OHT to inactivate Pu.1. At 26 dpi, the 4-OHT-treated fish were then injected 5 doses (one dose daily) of BrdU and the brain samples were collected 1 day later for TUNEL and BrdU staining respectively (Fig. 4A). Quantification results showed that the percentage of TUNEL^{+}DsRed^{+} microglia (*pu.1*-deficient cells) in the brains of the *pu.1*$^{KI/\Delta 839}$*;Tg(coro1a:CreER)* fish was significantly higher than that of TUNEL^{+}eGFP^{+} cells (Fig. 4B). In this assay, the 4-OHT-treated *pu.1*$^{KI/+}$*;Tg(coro1a:CreER)* fish were included as the control, and as expected, the percentages of TUNEL^{+} cells in the DsRed^{+} and eGFP^{+} microglia pools in control fish were comparable (Fig. 4B). In parallel, we also found that the BrdU incorporation rates of *pu.1*-deficient microglia (DsRed^{+}) in the 4-OHT-treated *pu.1*$^{KI/\Delta 839}$*;Tg(coro1a:CreER)* fish was significantly lower than that of eGFP^{+} cells (Fig. 4C), while the BrdU incorporation rates of DsRed^{+} cells and eGFP^{+} cells in the control *pu.1*$^{KI/+}$*;Tg(coro1a:CreER)* fish was comparable (Fig. 4C). These results indicate that conditional inactivation of Pu.1 in adult zebrafish leads to the impairment of cell proliferation and accelerated cell death of microglia in mosaic condition. To estimate the cell death and proliferation rates of microglia in *pu.1*-null mutants, we utilized a similar strategy via pulsing the adult *pu.1*$^{\Delta 839/+}$*;TgBAC(ccl34b.1:eGFP) or pu.1*$^{\Delta 839/\Delta 839}$*;TgBAC(ccl34b.1:eGFP)* fish with 5 doses of BrdU (daily) and collecting the brains samples at 1 day later for TUNEL and BrdU staining respectively (Fig. 4D). As shown in Fig. 4E, the percentage of TUNEL^{+}ccl34b.1-eGFP^{+} microglia showed no difference between *pu.1*$^{\Delta 839/\Delta 839}$ mutants and *pu.1*$^{\Delta 839/+}$ siblings, demonstrating that the intrinsic viability of *pu.1*-deficient microglia in the null mutants was largely unaffected. Similarly, the proliferation capability (as indicated by BrdU incorporation rate) of *pu.1*-deficient microglia in the null mutants remained normal as well in comparison with control siblings (Fig. 4F). Collectively, these results strongly suggest that the chronic elimination of *pu.1*-deficient DsRed^{+} microglia is indeed caused by cell competition, which only occurs in the mosaic condition when the eGFP^{+} microglia harboring a single copy of *pu.1* are present.

The out-competition of _pu.1_-deficient microglia in mosaic condition is mediated by Tp53

To uncover the key downstream targets that mediate the out-competition of *pu.1*-deficient DsRed^{+} microglia in mosaic condition, we manually picked DsRed^{+} and eGFP^{+} microglia from the 4-OHT-treated *pu.1*$^{KI/\Delta 839}$*;Tg(coro1a:CreER)* fish at 3 mpi and performed transcriptomic analysis (Fig. 5A). To minimize the contamination of DCs, we manually picked 3~5 DsRed^{+} or GFP^{+} cells from the brain suspension of 3-mpi *pu.1*$^{KI/\Delta 839}$*;Tg(coro1a:CreER)* fish in each tube for cDNA library construction and RNAseq. Samples with strong expression of microglia-related genes and faint DC-related genes were chosen for further analysis (Fig. S8A). Among the differential expressed genes (DEGs), the tumor suppressor gene *tp53* was one of the top targeted genes robustly upregulated in *pu.1*-deficient DsRed^{+} microglia (Fig. 5B-C, Fig. S8B). Interestingly, recent studies have revealed that, in addition to regulating cell cycle arrest and apoptosis in DNA damage response (Ou & Schumacher, 2018, Vaddavalli & Schumacher, 2022), Tp53 is also involved in cell competition regulation in both hematopoietic and non-hemopoietic tissues (Bondar & Medzhitov, 2010, Zhang, Xie et al., 2017). Hence, we speculated that the cell competition-mediated chronic elimination of *pu.1*-deficient microglia was likely dependent on Tp53. To support this hypothesis, we conditional inactivated Pu.1 to generate mosaic microglia populations in the *tp53*-deficient mutant background and asked if loss of Tp53 could rescue the microglia phenotype (Fig. 5D, upper panel). Indeed, results showed that the number of *pu.1*-deficient DsRed^{+} microglia in the 4-OHT-treated *pu.1*$^{KI/\Delta 839}$*;tp53*$^{-/-}$*;Tg(coro1a:CreER)* fish was significantly restored compared with *pu.1*$^{KI/\Delta 839}$*;Tg(coro1a:CreER)* control fish (Fig. 5D-F). Collectively, these results demonstrate that the chronic elimination of *pu.1*-deficient microglia in mosaic condition is mediated, at least in part, by the elevation of Tp53 activity, which leads to the reduced proliferation and excessive death of these microglia.

Dosage-dependent regulation of microglia maintenance by PU.1 is evolutionarily conserved from zebrafish to mice

The above data have demonstrated that the long-term maintenance of microglia in adult zebrafish is regulated by Pu.1 in a dosage-dependent manner. We next wondered whether this mechanism is evolutionarily conserved from teleost to mammals. To address this issue, we first examined the expression of *Pu.1* (Ensembl: ENSMUSG00000002111) and *Spi-b* (Ensembl: ENSMUSG00000008193) in adult murine microglia. Quantitative RT-PCR revealed that in contrast to the robust expression of *Pu.1*, *Spi-b* was barely detectable in microglia (Fig. S9A). It appears that *Spi-b* has acquired lineage specific roles during evolution and becomes absent in murine microglia. We therefore only focused on *Pu.1* and generated a *Pu.1*^{Fl} allele, in which the exon 2 of *Pu.1* gene is flanked by loxP (Fig. S9B-C). The *Pu.1*^{Fl} mice were then crossed with the *Cx3cr1*$^{CreER\text{-}YFP}$ strain

(referred to as to *Cx3cr1*^{CreER} hereafter) (Yona, Kim et al., 2013) to generate *Pu.1*$^{Fl/+}$*;Cx3cr1*^{CreER} and *Pu.1*$^{Fl/Fl}$*;Cx3cr1*^{CreER} mice for conditional PU.1 inactivation study (Fig. 6A).

To investigate whether microglia maintenance in adult mice requires PU.1, we intraperitoneally injected tamoxifen (TAM) (Askew et al., 2017) into the *Pu.1*$^{Fl/+}$*;Cx3cr1*^{CreER} *and Pu.1*$^{Fl/Fl}$*;Cx3cr1*^{CreER} mice, and collected the brain samples at 7 dpi for cryo-section and IBA1 staining (Fig. 6A, upper panel). As expected, without TAM, the number of the IBA1^{+} microglia showed no difference in the brain of *Pu.1*$^{Fl/+}$*;Cx3cr1*^{CreER} *and Pu.1*$^{Fl/Fl}$*;Cx3cr1*^{CreER} mice (Fig. S9D-E). However, after TAM injection, the number of the IBA1^{+} microglia in *Pu.1*$^{Fl/Fl}$*;Cx3cr1*^{CreER} mice were drastically reduced compared to that in *Pu.1*$^{Fl/+}$*;Cx3cr1*^{CreER} mice (Fig. 6A-C), suggesting that PU.1 is indeed required for the survival of adult microglia, which is similar to the double depletion of *pu.1* and *spi-b* in zebrafish (Fig. S5). To further explore whether partial loss of PU.1 activity could reduce the competitiveness of microglia and impairs the long-term maintenance of microglia in mice, we intraperitoneally injected sub-dosage of TAM into adult *Pu.1*$^{Fl/+}$*;Cx3cr1*^{CreER} mice to generate mosaic microglia populations for long-term tracing. To quantify the proportion of *Pu.1*$^{KO/+}$ microglia and *Pu.1*$^{Fl/+}$ microglia, we sorted YFP^{+} microglia from TAM-injected *Pu.1*$^{Fl/+}$*;Cx3cr1*^{CreER} mice at 3 dpi and 3.5 mpi, the timeline similar to previous research in zebrafish. Then we amplified *Pu.1*^{KO} and *Pu.1*^{Fl} alleles in the gDNA pool by PCR for T-clone quantification (Fig. 6D). As shown in Fig. 6E-F, while the percentage of *Pu.1*$^{KO/+}$ microglia was comparable to *Pu.1*$^{Fl/+}$ microglia at 3 dpi, it was dramatically reduced by 3.5 mpi, suggesting that removal of a single copy of *Pu.1* leads to the chronic elimination of *Pu.1*$^{KO/+}$ microglia, which appears to occur only in the presence of the WT *Pu.1*$^{Fl/+}$ microglia, as PU.1 heterozygous mice show no difference in the viability of tissue resident macrophages (Karpurapu et al., 2011). Collectively, these results indicate that the dosage-dependent cell competition-mediated regulation of microglia maintenance by SPI1/PU.1 is evolutionarily conserved from teleost to mammals.

Discussion

In the present study, to explore the role of Pu.1 in microglia survival and maintenance, we established a visible conditional knockout *pu.1*^{KI} allele in zebrafish via the non-homologous end joining (NHEJ)-mediated knock-in method. Although conditional inactivation of targeted genes has been reported by several independent studies (Li et al., 2015, Li, Zhang et al., 2019, Shin, Yin et al., 2023), it has not been widely applied in zebrafish, possibly due to the difficulty or low efficiency to generate loxP-flanked alleles. Compared to homologous recombination (HR), NHEJ-mediated knock-in of reporter gene has been shown to display 10-fold higher efficiency (Auer, Duroure et al., 2014, Li et al., 2015). In our case, the germline transmission to F1 generation for *pu.1*^{KI} allele is

around 15% (Fig. S1). Meanwhile, in our investigation, we noted that the efficiency of Cre-mediated excision of loxP sites at the *pu.1* locus in zebrafish (Fig. 3) appears much lower than that in mouse (Fig. 6). Although it remains to be further validated whether this observation is a general phenomenon, it does highlight the necessity and significance of chimera study of interested genes. In our $pu.1^{KI}$ allele, the expression of DsRed directly indicates Cre-mediated excision and helps us distinguish the mutant cells from their sibling cells, which serves as a good example for chimera study in the future. Moreover, our knock-in allele can also be simply regarded as a loxP-flanked fluorescent reporter line, which not only facilitates the labeling of cells that express gene of interest, but also can be used in combination with the LEGO-IR system (Xu et al., 2015) to trace the fate of these cells. Thus, due to the high integration efficiency of donor DNA fragment and the multifaceted applications of the labeling strategy, we anticipated that our knock-in system would be a powerful tool and broadly adopted in the fields of genetics, developmental biology and cell biology for the chimeric study of interested genes and fate mapping of interested cells in the future.

Via EdU pulse-chase labelling assay, we found that the daily turnover rate of microglia in adult zebrafish is about 2.5%, much higher than that reported in mice and human (Lopez-Atalaya, Askew et al., 2018). These disparities might be explained by several reasons. First, in our calculation of microglia turnover rate, we did not factor the unknown cell cycle length of zebrafish microglia. It is possible that the duration of microglia proliferation in zebrafish is much shorter than that in mice. If microglia proliferation takes less than 24 hours in zebrafish, then the calculated daily turnover rate of 2.5% may be overestimated. Second, it is well recognized that zebrafish manifest much stronger regeneration capability than mammals. As such, differentiated cells, like cardiomyocytes and hair cells in zebrafish are in general more proliferative than those in mammals (Chen, Zhang et al., 2019, Marques, Lupi et al., 2019). In this regard, microglia in zebrafish might be pre-coded both genetically and epigenetically to be more proliferative. Finally, microglia turnover could potentially be affected by the distinct efferocytotic burdens via the lysosome pathway, as lysosome has been known to be a convergent point for many biological process, including metabolism, cellular senescence, DNA repair, ER stress and even apoptosis (Franco-Juárez, Coronel-Cruz et al., 2022, Perera & Zoncu, 2016). Indeed, efferocytosis of apoptotic cells has previously been shown to elicit NOX2 assembly and promote ROS production (Yvan-Charvet, Pagler et al., 2010), which in turn triggers cell death via induction of lysosome damage (Patra, Patil et al., 2023, Wang, Gómez-Sintes et al., 2018). The more regenerative environment in zebrafish might be accompanied by higher frequency of cell death, which could lead to the increase of efferocytotic burdens of microglia, thereby accelerating the turnover of microglia. Further studies will be required to clarify this issue.

Our results revealed that the survival and maintenance microglia are highly sensitive to the dosage of PU.1/SPI1 in both teleost and mammals. Interestingly, a previous study reported that

hetero- or homozygosity of PU/ER(T) allele, in which the estrogen receptor (ER) ligand binding domain-G525R is fused with the full-length PU.1 to block its nuclear translocation, showed no effect on the viability of alveolar macrophages (Karpurapu et al., 2011). This contradictory result might potentially result from the leakiness of ER, which was incapable to fully retain PU.1 in cytoplasm. A recent work found that conditional inactivation of PU.1 by feeding the animals with tamoxifen-containing diet in the Alzheimer's disease model CK-p25 mice led to a 33% reduction in microglia number at their young ages. Although the authors considered prevention of microgliosis as a result of the amelioration of neuroinflammation (Ralvenius et al., 2023), our data implies that reduction in microglia could also been interpreted by the direct involvement of PU.1 in microglia survival and maintenance, as our data clearly demonstrate that conditional ablation of the PU.1 in mice or Pu.1/Spi-b in zebrafish leads to the rapid depletion of microglia in the brain (Fig. 6; Fig. S5). As PU.1 is a master regulator that controls the expression of series of genes required for macrophage/microglia development (Satoh et al., 2014), rapid death of *Pu.1*-null microglia might probably be caused by the orchestration of multiplex factors, including the downregulation of colony-stimulating factor 1 receptor (*Csf1r*) (the essential regulator controlling the survival and maintenance of microglia in both mice and zebrafish) (Elmore et al., 2014, Yu et al., 2023), the loss of anti-apoptotic genes, such as BCL2A1 (Jenal, Batliner et al., 2010), and absence of other genes that maintain the integrity of cells. Intriguingly, differing from the rapid death of microglia after complete inactivation of PU.1 or Pu.1/Spi-b, microglia with a partial loss of PU.1 or Pu.1 are chronically eliminated only in the mosaic condition via cell competition, in which the microglia with WT *Pu.1* or a single copy of *pu.1* are present (Fig. 3 and Fig. 6). Moreover, we further showed that the chronic elimination of *pu.1*-deficent microglia in zebrafish is mediated by Tp53-dependent cell competition, which has been shown to depend on the relative level of Tp53 in competing cells (Bondar & Medzhitov, 2010, Zhang et al., 2017). A previous study by Tschan et al has shown that PU.1 attenuates the transcriptional activity of the *p53* tumor suppressor family through direct binding to the DNA-binding and/or the oligomerization domains of p53/p73 proteins (Tschan, Reddy et al., 2008). Via in-silico analysis of *tp53* promoter region in zebrafish, we also found three PU.1 binding sequences (GAGGAA) located on antisense strand from position -1047 to -1042, -1098 to -1093 and -1423 to -1418 relative to the transcriptional start site of the *tp53* promoter (Fig. S10). These observations indicate that Pu.1 might regulate the activity of P53 through direct protein-protein or protein-DNA interactions. Previously, we have shown that the level of *csf1ra*, the zebrafish orthologue of mammalian *Csf1r*, is highly associated with the fitness of microglia and regulates the turnover and maintenance of microglia via cell-competition (Yu et al., 2023). During the process of investigation, we also wondered whether the cell competition between *pu.1*-deficient microglia and *pu.1*-sufficient microglia relied on Csf1ra. However, in contrast to the robust

upregulation of *p53* in *pu.1*-deficient microglia, the decrease of *csf1ra* was not observed (Fig. S11). In summary, our findings suggest that the dosage of PU.1/Pu.1 may serve as a checkpoint to determine the fitness of microglia. It will be of great interest to explore the upstream events that modulate *PU.1*/*pu.1* expression during microglia turnover.

Materials and Methods

Zebrafish

Zebrafish were maintained according to standard protocol as described previously (Westerfield, 2000). AB wild-type, *pu.1*$^{\Delta 839}$ (Yu et al., 2017), *spi-b*$^{\Delta 232}$ (Yu et al., 2017), *tp53*^{M214K} (Berghmans, Murphey et al., 2005), *pu.1*^{KI} (short for *pu.1*^{KI}-eGFP), *pu.1*^{CKO} (short for *pu.1*^{KI}-DsRed), *TgBAC(ccl34b.1:eGFP)* (Wu et al., 2020), *Tg(coro1a:CreER*^{T2}*)*^{sz101tg}, *Tg(mpeg1:loxP-DsRedx-loxP-eGFP, shorted as LRLG)*^{hkz015t} (Xu, Wang et al., 2016) were used in this study.

Mouse strains

Pu.1^{Fl} (No.T010980, purchased from GemPharmatech Co.,Ltd) and *Cx3cr1*$^{CreER\text{-}EYFP}$ (Stock No. 021160) (Yona et al., 2013) were used in this study. All animal experiments and procedures were proved by Ethics Committee for the Welfare of Laboratory Animals in Shenzhen PKU-HKUST Medical Center.

Generation of *pu.1*^{KI} allele

Donor plasmid was modified based on the reported Th-KI plasmid (Li et al., 2015). In brief, DNA fragments containing *pu.1* exon 4 to exon 6 and the 3' downstream fragment were cloned from cDNA and genomic DNA libraries respectively and inserted into the plasmid containing P2A-eGFP, P2A-Dsred and loxP elements. sgRNA was designed in the intron 3~4 of *pu.1* with the online website Crisprscan (https://www.crisprscan.org/). It was transcribed by MEGAshortscript Kit (AM1354, Invitrogen) from PCR product which was amplified following reported protocol (Vejnar, Moreno-Mateos et al., 2016). Then Cas9 mRNA (700 ng/ul), sgRNA (70 ng/ul) and donor plasmid (15 ng/ul) were mixed and injected into zebrafish embryos at one-cell stage. Embryos with eGFP signal were selected at 3 dpf and raised to adulthood for germline transmission. Adult F0 fish were crossed with wild-type fish to generate F1 and eGFP^{+} F1 were selected. The 5'- and 3'-junctions of the donor plasmid integration site were amplified from the genomic DNA of F1 embryos and sent for sequencing. The primers used for 5' junction are 5'-GATCTATCGACCACCAATGGAG-3' and 5'-GCCATAGTGTGCATTCTCAGG-3' and for 3' junction are 5'-GTTGTAAAACGACGGCCAG-3' and 5'-GAGTGTAGTGCTCATTCAAGC-3'.

Cryo-section

Adult fish were anesthetized on ice. The tissue was dissected and fixed in 4% PFA at 4□ overnight. After being washed with phosphate-buffered saline (PBS) at room temperature for 1 day, the tissues were dehydrated with 30% sucrose at 4□ overnight, then soaked in coagulating solution (optimal cutting temperature compound, OCT) and subjected to cryosection with 30-μm thickness.

EdU and BrdU incorporation assays, TUNEL staining, and immunostaining

EdU and BrdU incorporation assays were conducted as previously reported (Yu et al., 2023). In brief, EdU (A10044, Invitrogen) or BrdU (B5002, Sigma-Aldrich) was dissolved in PBS to the final concentration of 10 mg/ml. 5 ul EdU or BrdU was intraperitoneally (i.p.) injected into adult zebrafish each time. Brain samples were dissected at 1 day post injection and fixed in 4% PFA for cryosection.

EdU detection was conducted with (Click-iT™ EdU Cell Proliferation Kit for Imaging, Alexa Fluor™ 647 dye, Invitrogen, C10340) according to the manufacturer's instructions. For BrdU detection, samples were treated with 2M HCl for half an hour and then stained with the BrdU antibody. TUNEL staining was performed with TUNEL BrightGreen Apoptosis Detection Kit (A112, Vazyme) according to the manufacturer's instructions. Antibody staining was performed after EdU/BrdU and TUNEL detection. Primary antibodies used in this study were mouse anti-BrdU (11170376001, Roche), goat anti-GFP (ab6658, Abcam), rabbit anti-DsRed (632496, Clontech), rabbit anti-Lcp1 (Jin, Sood et al., 2009), rabbit anti-Pu.1 (Jin, Li et al., 2012) and rabbit anti-IBA1 (019-19741, FUJIFILM Wako) antibodies.

Tamoxifen injection

4-Hydroxytamoxifen (4-OHT, H7904, Sigma) was dissolved in ethanol to final concentration of 10 mM. For adult fish, 1 ul 4-OHT was i.p. injected into each fish for 3 times. For adult mice, tamoxifen (T5648, Sigma) was dissolved in corn oil to final concentration of 20 mg/ml and i.p. injected into the mice with 35 mg/kg (sub-dosage) or 150 mg/kg (over-dosage).

Neutral red staining

Neutral red staining was performed as previously described (Herbomel, Thisse et al., 2001).

Cy5-Annexin V treatment

Annexin V-Cy5 Reagent (1013, Biovision) solution was directly injected into brain ventricle of 3 dpf larva and immediately imaged by confocal microscope.

Imaging

Fluorescent signals from live reporter lines or immunostaining were imaged under a Leica SP8 confocal microscope or a Zeiss LSM980 confocal microscope. The objectives HC PL APO 203/0.70 DRY (Leica) and Plan-Apochromat 20×/0.8 M27 (Zeiss) were used in this study.

cDNA preparation and RNA-seq

Cell suspensions were prepared as previously described (Yu et al., 2017). Cells of interest were manually picked under the fluorescent microscope (Nikon Ti-S) equipped with the micro-manipulator (NT-88-V3, Nikon). Subsequently, picked cells were transferred by the glass needle to lysis buffer (mainly including Triton X-100 and RNase inhibitor) for thorough vertex. Then the cell lysate was used for reverse-transcription and amplification with the Smart-Seq2 method (Picelli, Faridani et al., 2014) to generate the cDNA library. cDNA was sent to Novogene Company for Illumina sequencing with an average depth of 6×10^6 raw reads per sample. Reads were aligned to the Zebrafish Genome Assembly GRCz11 using the STAR (Spliced Transcripts Alignment to a Reference). Original counts were calculated with featureCounts package. Differential expression genes (DEGs) were identified with the DESeq2 package. TPM (transcripts per million) are used to measure gene expression levels by normalization of counts. Samples with strong expression of microglia-related genes and faint DC-related genes were chosen for further analysis. TPM of top 50 up and down regulated genes were used to generate a heat map. TPM values in the heatmap were centered and scaled in the row direction. Noted that across all experimental groups subjected to RNA-seq analysis, the *ccl34b.1/ccl19a.1* expression ratios exceeded 5. Although residual DC contamination in the RNA-seq data cannot be entirely ruled out, we believed that microglia were the major population we analyzed in the RNA-seq.

Mouse microglia isolation

Adult mice brain was dissected and cut into small pieces. They were dissociated into single-cell suspensions with Adult Brain Dissociation Kit (130-107-677, Miltenyi Biotec) according to the manufacturer's instructions. Then Myelin Removal Beads II (130-96-733, Miltenyi Biotec) were used to remove myelin debris from single-cell suspensions. YFP^+ Microglia were sorted from suspensions by FACS Aria IIIu. The sorted microglia were lysed by proteinase K to extract DNA or TRIzol to extract RNA.

TA clone assay

$Pu.1^{Fl}$ and $Pu.1^{KO}$ alleles were amplified by PCR from the genomic DNA. The common forward primer was 5'-GCATCGCATTGTCTGAGTAGGT-3. The reverse primers were 5'-

AAATCTGCCTGGGTGACCTTC-3' for *Pu.1*^{Fl} and 5'-ACACAACGGGTTCTTCTGTTAG-3' for *Pu.1*^{KO}. The PCR products for *Pu.1* ^{Fl} and *Pu.1* ^{KO} alleles were 248 bp and 129 bp respectively. PCR products were ligated to pUCm-T vector (B522211, Sangon) with Blunt/TA Ligase Master Mix (M0367S, NEB) according to the manufacturer's instructions. The clones containing ligated plasmids were amplified with M13F (5'-GTTGTAAAACGACGGCCAG-3') and M13R (5'-CAGGAAACAGCTATGAC-3'). The PCR products for *Pu.1* ^{Fl} and *Pu.1* ^{KO} alleles were 437 bp and 315 bp respectively. Clones of *Pu.1*^{Fl} and *Pu.1*^{KO} alleles were distinguished by the size of PCR products.

Quantitative PCR

cDNA was synthesized from extracted RNA with SuperScript™ III Reverse Transcriptase kit (18080093, Invitrogen). Quantitative PCR was performed with iTaq™ Universal SYBR® Green Supermix (1725121, Bio-rad) on a CFX96 Dx Instrument (Bio-rad) and analyzed using the ΔΔCt method. The following primers were used to determine the expression of *DsRed* and *pu.1* from *pu.1*^{CKO} allele: *DsRed*, 5'-GATCTATCGACCACCAATGGAG-3' (*pu.1*-161FP)/ 5'-GCCGTTCACGGAGCCCTCCAT-3' (DsRed-72RP); *pu.1*, 5'-GATCTATCGACCACCAATGGAG-3' (*pu.1*-161FP)/ 5'-CGCATGTAGTGACTGCACGC-3' (*pu.1*-357RP). The following primers were used to determine the expression of *Pu.1* and *Spi-b* in mouse microglia: *Gapdh*, 5'-TGTGTCCGTCGTGGATCTGA-3'/5'-TTGCTGTTGAAGTCGCAGGAG-3'; *Pu.1*, 5'-GAGGTGTCTGATGGAGAAGCTG-3'/5'-ACCCACCAGATGCTGTCCTTCA-3'; *Spi-b*, 5'-AGGAGTCTTCTACGACCTGGAC-3'/5'-GGAGTGGCTAAAGGCAGCAGTA-3'.

Quantification and Statistics

The number microglia in embryos were quantified manually, and then genotyped to prevent bias. For the experiment with adults, fish were genotyped first and then numbered without gender bias for downstream 4-OHT injection, brain sample collection, cryo-section and immunostaining experiments. For microglia number quantification, 3 representative slices from anterior, middle and posterior of the midbrain of numbered fish were chosen for further manual counting with the same criterial. For EdU/BrdU or TUNEL experiments, at least 6 representative slices from anterior, middle and posterior of the midbrain were chosen for calculation. The number of EdU/BrdU^{+} or TUNEL^{+} microglia/DCs from the slices were counted and then divided by the total number of microglia/DCs to calculate the ratio.

Adult mice were genotyped first and then only males were chosen for the downstream experiments. Female mice were excluded to avoid variability associated with estrous cycle-dependent hormonal changes, which are known to influence microglial behavior (Habib & Beyer,

2015). For statistics, cortex, hippocampus and thalamus on the slices of mouse brain were chosen for microglia density quantification. The number of microglia and region of interest were calculated with Imaris 9.9 software to determine the density.

Statistical analyses are performed with Graphpad Prism 9.5.1. F test was first used to check the variances of two groups. If the variances of two groups were not significantly different ($P>0.05$), Student's t test was performed. If the variances of the two groups were significantly different ($P<0.05$), t test with Welch's correction was performed. A result was considered significant if $P<0.05$. Values represent mean ± standard deviation of the mean.

Funding

This work is supported by National Natural Science Foundation of China Grant (31801211), Natural Science Foundation of Guangdong Province Grant (2024A1515030122), Shenzhen Medical Academy of Research and Translation (SMART) 2023 Shenzhen Medical Research Funding (B2302034), and Research Grants Council of the Hong Kong Special Administrative Region Grants (16103920, AoE/M-09/12, T13-605/18-W, and T13-602/21-N).

Acknowledgements

We thank Dr. Keng Chen and Dr. Keyu Chen in Shenzhen Bay Laboratory for their assistance in the Fluorescent-activated cell sorting (FACS) of mouse microglia, and thank Prof. Jin Xu in South China University of Technology for his kind suggestions on this project.

References

Ajami B, Bennett JL, Krieger C, Tetzlaff W, Rossi FMV (2007) Local self-renewal can sustain CNS microglia maintenance and function throughout adult life. *Nature neuroscience* 10: 1538-1543

Askew K, Li K, Olmos-Alonso A, Garcia-Moreno F, Liang Y, Richardson P, Tipton T, Chapman MA, Riecken K, Beccari S, Sierra A, Molnár Z, Cragg MS, Garaschuk O, Perry VH, Gomez-Nicola D (2017) Coupled Proliferation and Apoptosis Maintain the Rapid Turnover of Microglia in the Adult Brain. *Cell Rep* 18: 391-405

Auer TO, Duroure K, De Cian A, Concordet JP, Del Bene F (2014) Highly efficient CRISPR/Cas9-mediated knock-in in zebrafish by homology-independent DNA repair. *Genome research* 24: 142-53

Berghmans S, Murphey RD, Wienholds E, Neuberg D, Kutok JL, Fletcher CDM, Morris JP, Liu TX, Schulte-Merker S, Kanki JP, Plasterk R, Zon LI, Look AT (2005) *tp53* mutant zebrafish develop malignant peripheral nerve sheath tumors. *Proceedings of the National Academy of Sciences* 102: 407-412

Bondar T, Medzhitov R (2010) p53-Mediated Hematopoietic Stem and Progenitor Cell Competition. *Cell Stem Cell* 6: 309-322

Bruttger J, Karram K, Wörtge S, Regen T, Marini F, Hoppmann N, Klein M, Blank T, Yona S, Wolf Y, Mack M, Pinteaux E, Müller W, Zipp F, Binder H, Bopp T, Prinz M, Jung S, Waisman A (2015) Genetic Cell Ablation Reveals Clusters of Local Self-Renewing Microglia in the Mammalian Central Nervous System. *Immunity* 43: 92-106

Cao H, Zhou X, Chen Y, Ip FCF, Chen Y, Lai NCH, Lo RMN, Tong EPS, Mok VCT, Kwok TCY, Fu AKY, Ip NY (2022) Association of SPI1 Haplotypes with Altered SPI1 Gene Expression and Alzheimer's Disease Risk. *J Alzheimers Dis* 86: 1861-1873

Chen Y, Zhang S, Chai R, Li H (2019) Hair Cell Regeneration. In *Hearing Loss: Mechanisms, Prevention and Cure*, Li H, Chai R (eds) pp 1-16. Singapore: Springer Singapore

Colonna M, Butovsky O (2017) Microglia Function in the Central Nervous System During Health and Neurodegeneration. *Annual Review of Immunology* 35: 441-468

Elmore Monica RP, Najafi Allison R, Koike Maya A, Dagher Nabil N, Spangenberg Elizabeth E, Rice Rachel A, Kitazawa M, Matusow B, Nguyen H, West Brian L, Green Kim N (2014) Colony-Stimulating Factor 1 Receptor Signaling Is Necessary for Microglia Viability, Unmasking a Microglia Progenitor Cell in the Adult Brain. *Neuron* 82: 380-397

Franco-Juárez B, Coronel-Cruz C, Hernández-Ochoa B, Gómez-Manzo S, Cárdenas-Rodríguez N, Arreguin-Espinosa R, Bandala C, Canseco-Ávila LM, Ortega-Cuellar D (2022) TFEB; Beyond Its Role as an Autophagy and Lysosomes Regulator. *Cells* 11: 3153

Füger P, Hefendehl JK, Veeraraghavalu K, Wendeln AC, Schlosser C, Obermüller U, Wegenast-Braun BM, Neher JJ, Martus P, Kohsaka S, Thunemann M, Feil R, Sisodia SS, Skodras A, Jucker M (2017) Microglia turnover with aging and in an Alzheimer's model via long-term in vivo single-cell imaging. *Nature neuroscience* 20: 1371-1376

Ginhoux F, Greter M, Leboeuf M, Nandi S, See P, Gokhan S, Mehler MF, Conway SJ, Ng LG, Stanley ER, Samokhvalov IM, Merad M (2010) Fate mapping analysis reveals that adult microglia derive from primitive macrophages. *Science* 330: 841-5

Glass CK, Saijo K, Winner B, Marchetto MC, Gage FH (2010) Mechanisms underlying inflammation in neurodegeneration. *Cell* 140: 918-34

Gomez-Nicola D, Perry VH (2015) Microglial Dynamics and Role in the Healthy and Diseased Brain: A Paradigm of Functional Plasticity. *The Neuroscientist* 21: 169-184

Habib P, Beyer C (2015) Regulation of brain microglia by female gonadal steroids. *J Steroid Biochem Mol Biol* 146: 3-14

Herbomel P, Thisse B, Thisse C (2001) Zebrafish early macrophages colonize cephalic mesenchyme and developing brain, retina, and epidermis through a M-CSF receptor-dependent invasive process. *Developmental biology* 238: 274-88

Huang KL, Marcora E, Pimenova AA, Di Narzo AF, Kapoor M, Jin SC, Harari O, Bertelsen S, Fairfax BP, Czajkowski J, Chouraki V, Grenier-Boley B, Bellenguez C, Deming Y, McKenzie A, Raj T, Renton AE, Budde J, Smith A, Fitzpatrick A et al. (2017) A common haplotype lowers PU.1 expression in myeloid cells and delays onset of Alzheimer's disease. *Nature neuroscience* 20: 1052-1061

Hughes AN, Appel B (2020) Microglia phagocytose myelin sheaths to modify developmental myelination. *Nature neuroscience* 23: 1055-1066

Iyer H, Shen K, Meireles AM, Talbot WS (2022) A lysosomal regulatory circuit essential for the development and function of microglia. *Sci Adv* 8: eabp8321

Jenal M, Batliner J, Reddy VA, Haferlach T, Tobler A, Fey MF, Torbett BE, Tschan MP (2010) The anti-apoptotic gene BCL2A1 is a novel transcriptional target of PU.1. *Leukemia* 24: 1073-6

Jin H, Li L, Xu J, Zhen F, Zhu L, Liu PP, Zhang M, Zhang W, Wen Z (2012) Runx1 regulates embryonic myeloid fate choice in zebrafish through a negative feedback loop inhibiting Pu.1 expression. *Blood* 119: 5239-49

Jin H, Sood R, Xu J, Zhen F, English MA, Liu PP, Wen Z (2009) Definitive hematopoietic stem/progenitor cells manifest distinct differentiation output in the zebrafish VDA and PBI. *Development* 136: 647-54

Karpurapu M, Wang X, Deng J, Park H, Xiao L, Sadikot RT, Frey RS, Maus UA, Park GY, Scott EW, Christman JW (2011) Functional PU.1 in macrophages has a pivotal role in NF-κB activation and neutrophilic lung inflammation during endotoxemia. *Blood* 118: 5255-5266

Kierdorf K, Erny D, Goldmann T, Sander V, Schulz C, Perdiguero EG, Wieghofer P, Heinrich A, Riemke P, Holscher C, Muller DN, Luckow B, Brocker T, Debowski K, Fritz G, Opdenakker G, Diefenbach A, Biber K, Heikenwalder M, Geissmann F et al. (2013) Microglia emerge from erythromyeloid precursors via Pu.1- and Irf8-dependent pathways. *Nature neuroscience* 16: 273-80

Lawson LJ, Perry VH, Gordon S (1992) Turnover of resident microglia in the normal adult mouse brain. *Neuroscience* 48: 405-15

Li J, Zhang BB, Ren YG, Gu SY, Xiang YH, Du JL (2015) Intron targeting-mediated and endogenous gene integrity-maintaining knockin in zebrafish using the CRISPR/Cas9 system. *Cell research* 25: 634-7

Li W, Zhang Y, Han B, Li L, Li M, Lu X, Chen C, Lu M, Zhang Y, Jia X, Zhu Z, Tong X, Zhang B (2019) One-step efficient generation of dual-function conditional knockout and geno-tagging alleles in zebrafish. *Elife* 8

Li Y, Du X-f, Liu C-s, Wen Z-l, Du J-l (2012) Reciprocal Regulation between Resting Microglial Dynamics and Neuronal Activity In Vivo. *Developmental cell* 23: 1189-1202

Lopez-Atalaya JP, Askew KE, Sierra A, Gomez-Nicola D (2018) Development and maintenance of the brain's immune toolkit: Microglia and non-parenchymal brain macrophages. *Dev Neurobiol* 78: 561-579

Marques IJ, Lupi E, Mercader N (2019) Model systems for regeneration: zebrafish. *Development* 146

McKercher SR, Torbett BE, Anderson KL, Henkel GW, Vestal DJ, Baribault H, Klemsz M, Feeney AJ, Wu GE, Paige CJ, Maki RA (1996) Targeted disruption of the PU.1 gene results in multiple hematopoietic abnormalities. *The EMBO journal* 15: 5647-58

Ou H-L, Schumacher B (2018) DNA damage responses and p53 in the aging process. *Blood* 131: 488-495

Patra S, Patil S, Klionsky DJ, Bhutia SK (2023) Lysosome signaling in cell survival and programmed cell death for cellular homeostasis. *Journal of Cellular Physiology* 238: 287-305

Perera RM, Zoncu R (2016) The Lysosome as a Regulatory Hub. *Annual Review of Cell and Developmental Biology* 32: 223-253

Peri F, Nüsslein-Volhard C (2008) Live Imaging of Neuronal Degradation by Microglia Reveals a Role for v0-ATPase a1 in Phagosomal Fusion In Vivo. *Cell* 133: 916-927

Picelli S, Faridani OR, Björklund ÅK, Winberg G, Sagasser S, Sandberg R (2014) Full-length RNA-seq from single cells using Smart-seq2. *Nature Protocols* 9: 171

Prinz M, Priller J, Sisodia SS, Ransohoff RM (2011) Heterogeneity of CNS myeloid cells and their roles in neurodegeneration. *Nature neuroscience* 14: 1227-35

Ralvenius WT, Mungenast AE, Woolf H, Huston MM, Gillingham TZ, Godin SK, Penney J, Cam HP, Gao F, Fernandez CG, Czako B, Lightfoot Y, Ray WJ, Beckmann A, Goate AM, Marcora E, Romero-Molina C, Ayata P, Schaefer A, Gjoneska E et al. (2023) A novel molecular class that recruits HDAC/MECP2 complexes to PU.1 motifs reduces neuroinflammation. *J Exp Med* 220

Satoh J, Asahina N, Kitano S, Kino Y (2014) A Comprehensive Profile of ChIP-Seq-Based PU.1/Spi1 Target Genes in Microglia. *Gene Regul Syst Bio* 8: 127-39

Schulz C, Gomez Perdiguero E, Chorro L, Szabo-Rogers H, Cagnard N, Kierdorf K, Prinz M, Wu B, Jacobsen SE, Pollard JW, Frampton J, Liu KJ, Geissmann F (2012) A lineage of myeloid cells independent of Myb and hematopoietic stem cells. *Science* 336: 86-90

Scott EW, Simon MC, Anastasi J, Singh H (1994) Requirement of transcription factor PU.1 in the development of multiple hematopoietic lineages. *Science* 265: 1573-7

Shin M, Yin HM, Shih YH, Nozaki T, Portman D, Toles B, Kolb A, Luk K, Isogai S, Ishida K, Hanasaka T, Parsons MJ, Wolfe SA, Burns CE, Burns CG, Lawson ND (2023) Generation and application of endogenously floxed alleles for cell-specific knockout in zebrafish. *Developmental cell* 58: 2614-2626.e7

Smith AM, Gibbons HM, Oldfield RL, Bergin PM, Mee EW, Faull RL, Dragunow M (2013) The transcription factor PU.1 is critical for viability and function of human brain microglia. *Glia* 61: 929-42

Su GH, Chen HM, Muthusamy N, Garrett-Sinha LA, Baunoch D, Tenen DG, Simon MC (1997) Defective B cell receptor-mediated responses in mice lacking the Ets protein, Spi-B. *The EMBO journal* 16: 7118-29

Tay TL, Mai D, Dautzenberg J, Fernández-Klett F, Lin G, Sagar, Datta M, Drougard A, Stempfl T, Ardura-Fabregat A, Staszewski O, Margineanu A, Sporbert A, Steinmetz LM, Pospisilik JA, Jung S, Priller J, Grün D, Ronneberger O, Prinz M (2017) A new fate mapping system reveals context-dependent random or clonal expansion of microglia. *Nature neuroscience* 20: 793-803

Tschan MP, Reddy VA, Ress A, Arvidsson G, Fey MF, Torbett BE (2008) PU.1 binding to the p53 family of tumor suppressors impairs their transcriptional activity. *Oncogene* 27: 3489-93

Vaddavalli PL, Schumacher B (2022) The p53 network: cellular and systemic DNA damage responses in cancer and aging. *Trends in Genetics* 38: 598-612

Vejnar CE, Moreno-Mateos MA, Cifuentes D, Bazzini AA, Giraldez AJ (2016) Optimized CRISPR-Cas9 System for Genome Editing in Zebrafish. *Cold Spring Harb Protoc* 2016

Walton MR, Gibbons H, MacGibbon GA, Sirimanne E, Saura J, Gluckman PD, Dragunow M (2000) PU.1 expression in microglia. *J Neuroimmunol* 104: 109-15

Wang F, Gómez-Sintes R, Boya P (2018) Lysosomal membrane permeabilization and cell death. *Traffic* 19: 918-931

Westerfield M (2000) The Zebrafish Book: A Guide for the Laboratory Use of Zebrafish (Danio rerio), 4th Edition. University of Oregon Press, Eugene.

Wu S, Nguyen LTM, Pan H, Hassan S, Dai Y, Xu J, Wen Z (2020) Two phenotypically and functionally distinct microglial populations in adult zebrafish. *Sci Adv* 6

Xu J, Wang T, Wu Y, Jin W, Wen Z (2016) Microglia Colonization of Developing Zebrafish Midbrain Is Promoted by Apoptotic Neuron and Lysophosphatidylcholine. *Developmental cell* 38: 214-222

Xu J, Zhu L, He S, Wu Y, Jin W, Yu T, Qu JY, Wen Z (2015) Temporal-Spatial Resolution Fate Mapping Reveals Distinct Origins for Embryonic and Adult Microglia in Zebrafish. *Developmental cell* 34: 632-41
Yona S, Kim K-W, Wolf Y, Mildner A, Varol D, Breker M, Strauss-Ayali D, Viukov S, Guilliams M, Misharin A, Hume David A, Perlman H, Malissen B, Zelzer E, Jung S (2013) Fate Mapping Reveals Origins and Dynamics of Monocytes and Tissue Macrophages under Homeostasis. *Immunity* 38: 79-91
Yu T, Guo W, Tian Y, Xu J, Chen J, Li L, Wen Z (2017) Distinct regulatory networks control the development of macrophages of different origins in zebrafish. *Blood* 129: 509-519
Yu T, Kuang H, Wu X, Huang Y, Wang J, Wen Z (2023) Cell competition for neuron-derived trophic factor controls the turnover and lifespan of microglia. *Sci Adv* 9: eadf9790
Yvan-Charvet L, Pagler TA, Seimon TA, Thorp E, Welch CL, Witztum JL, Tabas I, Tall AR (2010) ABCA1 and ABCG1 Protect Against Oxidative Stress–Induced Macrophage Apoptosis During Efferocytosis. *Circulation Research* 106: 1861-1869
Zhang G, Xie Y, Zhou Y, Xiang C, Chen L, Zhang C, Hou X, Chen J, Zong H, Liu G (2017) p53 pathway is involved in cell competition during mouse embryogenesis. *Proceedings of the National Academy of Sciences* 114: 498-503
Zhou Q, Zhao C, Yang Z, Qu R, Li Y, Fan Y, Tang J, Xie T, Wen Z (2023) Cross-organ single-cell transcriptome profiling reveals macrophage and dendritic cell heterogeneity in zebrafish. *Cell Reports* 42

Figure legends

Fig. 1. Adult microglia in zebrafish undergo rapid turnover and random proliferation to replenish and maintain their pool. (A) Schematic diagram shows the workflow of EdU pulse experiment in adult *TgBAC(ccl34b.1:eGFP)* zebrafish and the representative images of proliferating microglia (ccl34b.1-eGFP$^+$ Lcp1$^+$EdU$^+$) and dendritic cells (DCs) (ccl34b.1-eGFP$^-$Lcp1$^+$EdU$^+$) in the midbrain. **(B)** Quantification of the EdU incorporation proportions in microglia and DCs with different dosages of EdU pulses. (n=4 for each group) **(C)** The daily turnover rate of microglia and DCs calculated by dividing the EdU incorporation rate with EdU pulses. **(D)** Schematic diagram shows the experimental setup for EdU-BrdU double-pulse in adult wild-type fish and the representative images shows two BrdU$^+$ microglia with or without EdU incorporation. **(E)** Comparison of BrdU incorporation proportions in EdU$^+$eGFP$^+$ and EdU$^-$eGFP$^+$ microglia (n=6). n.s. = not significant, p>0.05.

Fig. 2. Generation and characterization of the visible conditional knockout allele *pu.1^{KI}*. (A) Schematic diagrams show the generation of *pu.1^{KI}* allele and the principle for *pu.1* visible conditional knockout. Briefly, the donor plasmid, which contains: (1) the sgRNA target sequence in *pu.1* intron 3~4; (2) the loxP-flanked *pu.1* coding sequence (exon4-6) followed by P2A-eGFP; (3) the splicing acceptor site followed by P2A-DsRed sequence was knocked into the endogenous *pu.1* locus via non-homologous end joining (NHEJ) to generate *pu.1^{KI}*. In principle, the splicing event occurring between E3 and E4 In *pu.1^{KI}* would produce intact Pu.1 and eGFP concurrently. After Cre-mediated recombination, removal of *pu.1* E4-6 and splicing of P2A-DsRed sequence in *pu.1^{CKO}* allele leads to the disruption of Pu.1 and fluorescent color change. **(B)** Co-staining of anti-eGFP and anti-Pu.1 antibodies on the yolk sac (YS) of 21-hpf *pu.1^{KI}* embryos. **(C)** Fluorescent imaging of the

753 optic tectum (OT) region of 3-dpf *pu.1*^{KI}*;Tg(mpeg1:LRLG)* embryos. **(D)** Co-staining of anti-eGFP
754 and anti-Lcp1 antibodies on the midbrain cross section of adult *pu.1*^{KI} fish. **(E)** Neutral red staining
755 of *pu.1*$^{KI/+}$ and *pu.1*$^{KI/\Delta 839}$ embryos at 3 dpf. **(F)** Quantification of NR^{+} microglia in *pu.1*$^{KI/+}$ (n=13)
756 and *pu.1* $^{KI/\Delta 839}$ (n=9) embryos at 3 dpf. **(G)** Fluorescent imaging of the YS region of 30-hpf
757 *pu.1*$^{KI/CKO}$ embryos. **(H)** Chromogram of cDNA sequence from wildtype and *pu.1*^{CKO} embryos
758 shows the precise splicing of *pu.1* E4 and *P2A-DsRed* cassette to *pu.1* E3. **(I)** Neutral red staining of
759 *pu.1*$^{CKO/+}$ and *pu.1*$^{CKO/\Delta 839}$ embryos at 3 dpf. **(J)** Quantification of NR^{+} microglia in *pu.1*$^{CKO/+}$ (n=8)
760 and *pu.1*$^{CKO/\Delta 839}$ embryos at 3 dpf (n=14). n.s. = not significant, p>0.05; ****p<0.0001.
761
762 **Fig. 3. *pu.1*-deficient microglia were chronically eliminated in mosaic condition. (A)** The
763 experimental setup for *pu.1* conditional knockout in adult zebrafish and the representative images of
764 midbrain cross section of *pu.1*$^{KI/+}$*;Tg(coro1a:CreER)* and *pu.1*$^{KI/\Delta 839}$*;Tg(coro1a:CreER)* fish at 8
765 days post 4-OHT injection (dpi). **(B)** Quantification of the number of DsRed^{+} microglia on the
766 midbrain cross section of *pu.1*$^{KI/+}$*;Tg(coro1a:CreER)* and *pu.1*$^{KI/\Delta 839}$*;Tg(coro1a:CreER)* fish at 2
767 dpi (n=3) and 8 dpi (n=4). **(C)** Quantification of the proportion of DsRed^{+} microglia on the
768 midbrain cross section of *pu.1*$^{KI/+}$*;Tg(coro1a:CreER)* and *pu.1*$^{KI/\Delta 839}$*;Tg(coro1a:CreER)* fish at 2
769 dpi (n=3) and 8 dpi (n=4). **(D)** The experimental setup for *pu.1* conditional knockout in adult
770 zebrafish and the representative images of midbrain cross section of *pu.1*$^{KI/+}$*;Tg(coro1a:CreER)* and
771 *pu.1*$^{KI/\Delta 839}$*;Tg(coro1a:CreER)* fish at 3 months post 4-OHT injection (mpi). **(E)** Quantification of
772 the number of DsRed^{+} microglia on the midbrain cross section of *pu.1*$^{KI/+}$*;Tg(coro1a:CreER)* and
773 *pu.1*$^{KI/\Delta 839}$*;Tg(coro1a:CreER)* fish at 1 mpi (n=3) and 3 mpi (n=4). **(F)** Quantification of the
774 proportion of DsRed^{+} microglia on the midbrain cross section of *pu.1*$^{KI/+}$*;Tg(coro1a:CreER)* and
775 *pu.1*$^{KI/\Delta 839}$*;Tg(coro1a:CreER)* fish at 1 mpi (n=3) and 3 mpi (n=4). n.s. = not significant, p>0.05;
776 **p<0.01; ****p<0.0001.
777
778 **Fig. 4. *pu.1*-deficient microglia in mosaic condition were eliminated by cell competition. (A)**
779 The experimental setup for BrdU incorporation and TUNEL assays in adult
780 *pu.1*$^{KI/+}$*;Tg(coro1a:CreER)* and *pu.1*$^{KI/\Delta 839}$*;Tg(coro1a:CreER)* fish at 1 mpi. **(B)** Quantification of
781 the percentage of TUNEL^{+} cells in eGFP^{+} and DsRed^{+} microglia in *pu.1*$^{KI/+}$*;Tg(coro1a:CreER)*
782 (n=4) and *pu.1*$^{KI/\Delta 839}$*;Tg(coro1a:CreER)* (n=5) fish at 1 mpi. **(C)** Quantification of the percentage
783 of BrdU^{+} cells in eGFP^{+} and DsRed^{+} microglia in adult *pu.1*$^{KI/+}$*;Tg(coro1a:CreER)* (n=4) and
784 *pu.1*$^{KI/\Delta 839}$*;Tg(coro1a:CreER)* fish at 1 mpi. **(D)** The experimental setup for BrdU incorporation and
785 TUNEL assays in adult *pu.1* $^{\Delta 839/+}$*;TgBAC(ccl34b.1:eGFP)* and
786 *pu.1*$^{\Delta 839/\Delta 839}$*;TgBAC(ccl34b.1:eGFP)* fish. **(E)** Quantification of the percentage of TUNEL^{+}eGFP^{+}

microglia in adult *pu.1*$^{\Delta 839/+}$*;TgBAC(ccl34b.1:eGFP)* and *pu.1*$^{\Delta 839/\Delta 839}$*;TgBAC(ccl34b.1:eGFP)* fish. **(F)** Quantification of the percentage of BrdU^{+}eGFP^{+} microglia in adult *pu.1*$^{\Delta 839/+}$*;TgBAC(ccl34b.1:eGFP)* (n=6) and *pu.1*$^{\Delta 839/\Delta 839}$*;TgBAC(ccl34b.1:eGFP)* (n=5) fish. n.s. = not significant, p>0.05; *p<0.05; **p<0.01.

Fig. 5. Inactivation of Tp53 largely restored the number of *pu.1*-deficient microglia in mosaic condition. (A) The experimental setup for the isolation of eGFP^{+} and DsRed^{+} microglia from *pu.1*$^{KI/\Delta 839}$*;Tg(coro1a:CreER)* adult brain at 3 mpi for transcriptomic analysis. **(B)** The volcano plot of differential expressed genes (DEG) between eGFP^{+} and DsRed^{+} microglia at 3 mpi. **(C)** Relative expression of *tp53* in eGFP^{+} (n=3) and DsRed^{+} (n=3) microglia at 3 mpi by transcripts per million (TPM). **(D)** The experimental setup for *pu.1* conditional knockout in wild-type and *tp53*$^{-/-}$ adult zebrafish, and the representative images of midbrain cross section of *pu.1*$^{KI/\Delta 839}$*;Tg(coro1a:CreER)* and *pu.1*$^{KI/\Delta 839}$*;tp53*$^{-/-}$*;Tg(coro1a:CreER)* fish at 3 mpi. **(E)** Quantification of the number of DsRed^{+}, eGFP^{+} and total (DsRed + eGFP) microglia in *pu.1*$^{KI/\Delta 839}$*;Tg(coro1a:CreER)* (n=7) and *pu.1*$^{KI/\Delta 839}$*;tp53*$^{-/-}$*;Tg(coro1a:CreER)* (n=6) fish at 3 mpi. **(F)** Quantification of the proportion of DsRed^{+} microglia in *pu.1*$^{KI/\Delta 839}$*;Tg(coro1a:CreER)* (n=7) *and pu.1*$^{KI/\Delta 839}$*;tp53*$^{-/-}$*;Tg(coro1a:CreER)* (n=6) fish at 90 dpi. n.s. = not significant, p>0.05; *p<0.05.

Fig. 6. Dosage-dependent regulation of microglia maintenance by Pu.1/Spi1 is evolutionary conserved in mice. (A) The experimental setup for *Pu.1* conditional knockout in adult mice. **(B)** Representative images of IBA1 and DAPI co-staining in the cortex, hippocampus and thalamus of *Pu.1*$^{Fl/+}$*;Cx3cr1*^{CreER} and *Pu.1*$^{Fl/Fl}$*;Cx3cr1*^{CreER} mice at 7 dpi. **(C)** Quantification of the density of IBA1^{+} microglia in the cortex, hippocampus and thalamus of *Pu.1*$^{Fl/+}$*;Cx3cr1*^{CreER} (n=3) and *Pu.1*$^{Fl/Fl}$*;Cx3cr1*^{CreER} (n=3) mice at 7 dpi. **(D)** The experimental setup for conditional knockout of *Pu.1* in *Pu.1*$^{Fl/+}$*;Cx3cr1*^{CreER} mice, and the subsequent PCR detection and T-clone quantification of *Pu.1*^{Fl} and *Pu.1*^{KO} alleles in sorted YFP^{+} microglia. **(E)** Gel image shows the relative intensity of amplified DNA bands of *Pu.1*^{Fl} and *Pu.1*^{KO} alleles in microglia sorted from *Pu.1*$^{Fl/+}$*;Cx3cr1*^{CreER} mice at different stages post TAM injection. (**F**) Quantification of the percentage of *Pu.1*^{KO} allele at 3 dpi (n=4) and 3.5 mpi (n=4) by T-clone assay. *p<0.05; **p<0.01; ***p<0.001; ****p<0.0001.

Figure 1

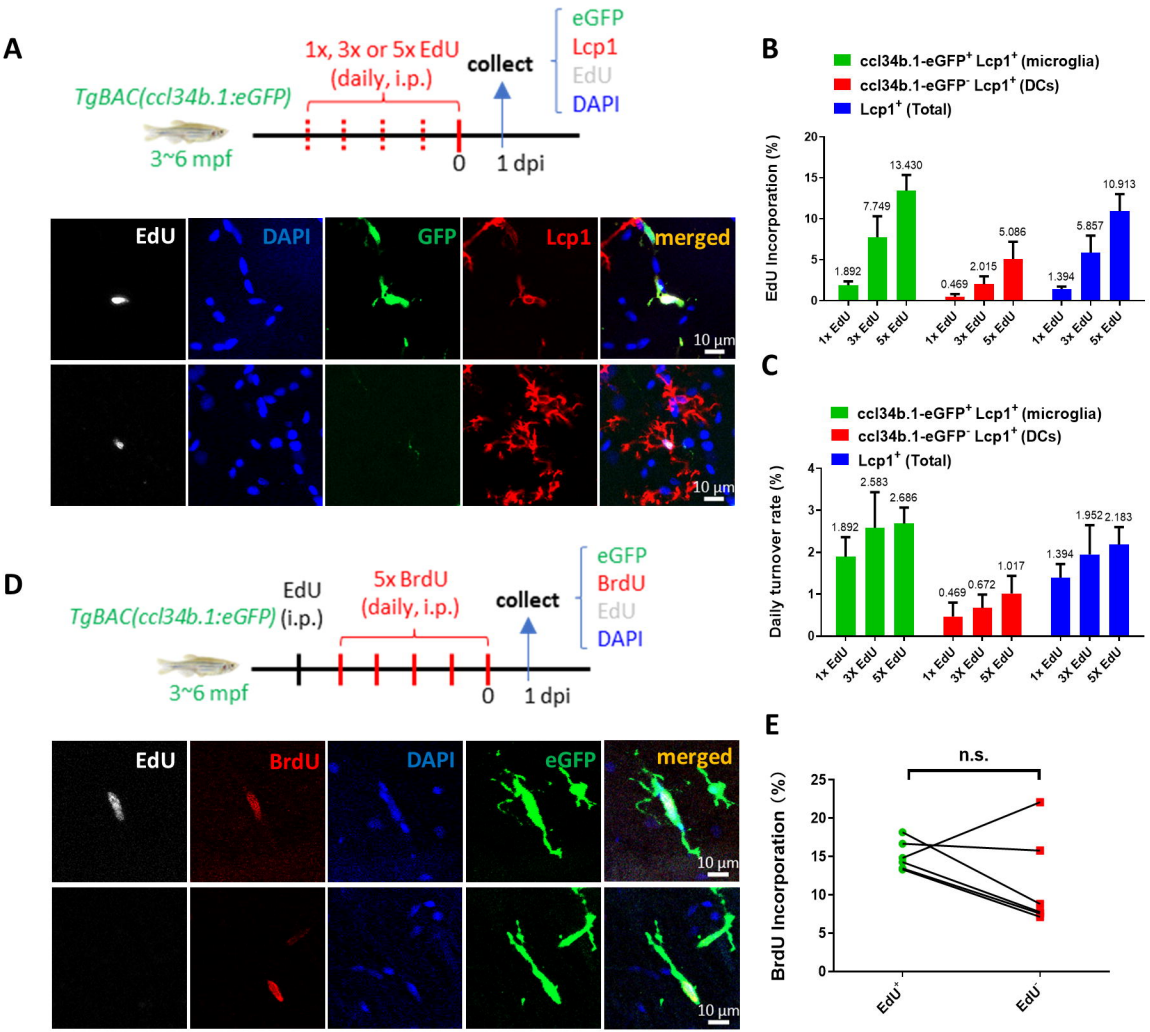
A
TgBAC(ccl34b.1:eGFP)
3~6 mpf
1x, 3x or 5x EdU
(daily, i.p.)
collect
0
1 dpi
eGFP
Lcp1
EdU
DAPI
EdU
DAPI
GFP
Lcp1
merged
10 μm
B
ccl34b.1-eGFP+ Lcp1+ (microglia)
ccl34b.1-eGFP- Lcp1+ (DCs)
Lcp1+ (Total)
EdU Incorporation (%)
1.892
7.749
13.430
0.469
2.015
5.086
1.394
5.857
10.913
1x EdU
3x EdU
5x EdU
C
ccl34b.1-eGFP+ Lcp1+ (microglia)
ccl34b.1-eGFP- Lcp1+ (DCs)
Lcp1+ (Total)
Daily turnover rate (%)
1.892
2.583
2.686
0.469
0.672
1.017
1.394
1.952
2.183
1x EdU
3X EdU
5X EdU
D
TgBAC(ccl34b.1:eGFP)
EdU
(i.p.)
3~6 mpf
5x BrdU
(daily, i.p.)
collect
0
1 dpi
eGFP
BrdU
EdU
DAPI
EdU
BrdU
DAPI
eGFP
merged
10 μm
E
n.s.
BrdU Incorporation (%)
EdU+
EdU-

Figure 2

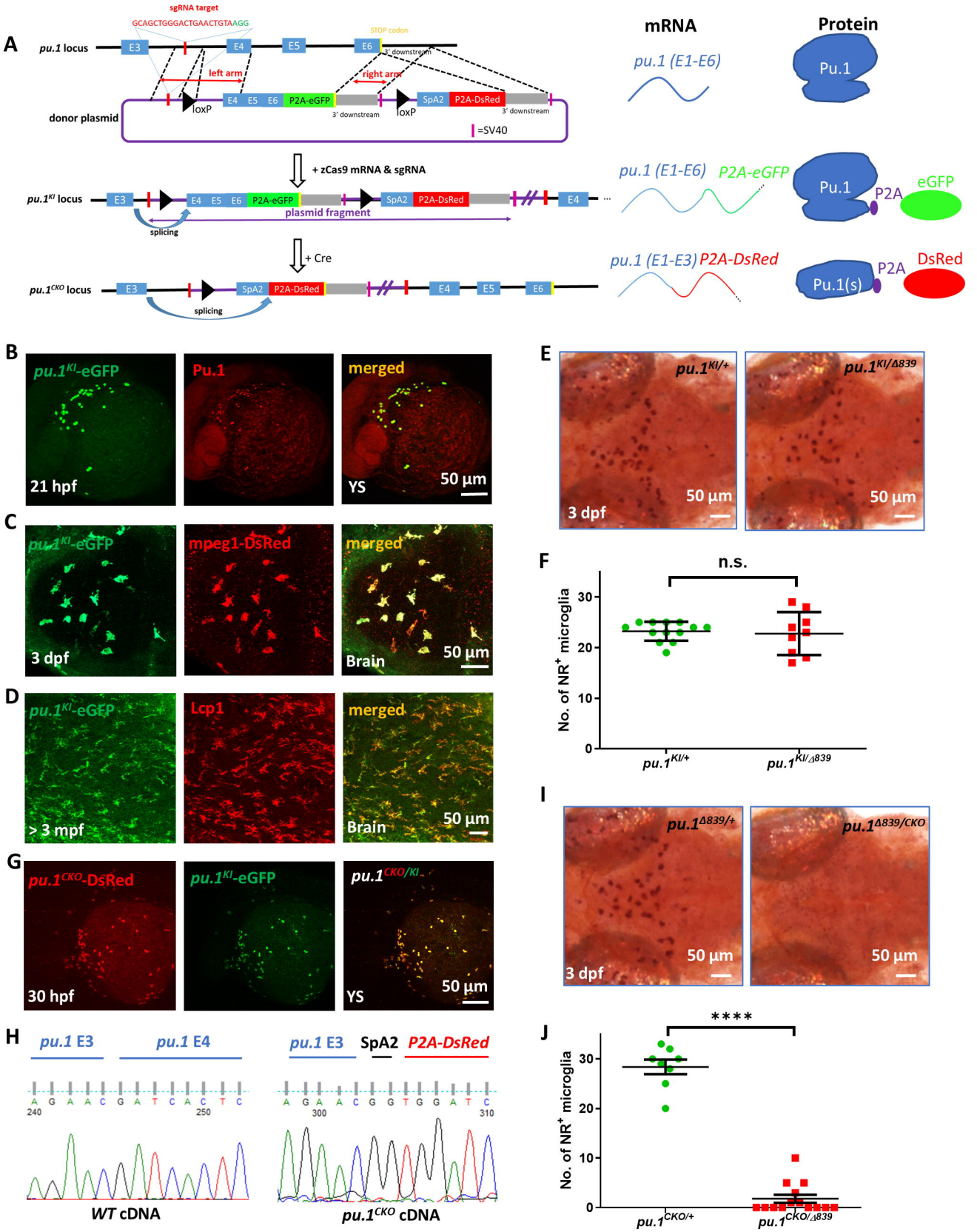
A
sgRNA target
GCAGCTGGGACTGAACTGTAAGG
STOP codon
pu.1 locus
E3
E4
E5
E6
3' downstream
left arm
right arm
donor plasmid
loxP
E4 E5 E6 P2A-eGFP
SpA2 P2A-DsRed
3' downstream
=SV40
+ zCas9 mRNA & sgRNA
pu.1KI locus
plasmid fragment
splicing
+ Cre
pu.1CKO locus
mRNA
Protein
pu.1 (E1-E6)
Pu.1
P2A-eGFP
P2A
eGFP
pu.1 (E1-E3)
P2A-DsRed
Pu.1(s)
DsRed
B
pu.1KI-eGFP
Pu.1
merged
21 hpf
YS
50 µm
C
mpeg1-DsRed
3 dpf
Brain
D
Lcp1
> 3 mpf
E
pu.1KI/+
pu.1KI/Δ839
F
n.s.
No. of NR+ microglia
pu.1KI/+
pu.1KI/Δ839
G
pu.1CKO-DsRed
pu.1CKO/KI
30 hpf
H
pu.1 E3
pu.1 E4
SpA2
P2A-DsRed
WT cDNA
pu.1CKO cDNA
I
pu.1Δ839/+
pu.1Δ839/CKO
J
****
pu.1CKO/+
pu.1CKO/Δ839

Figure 3

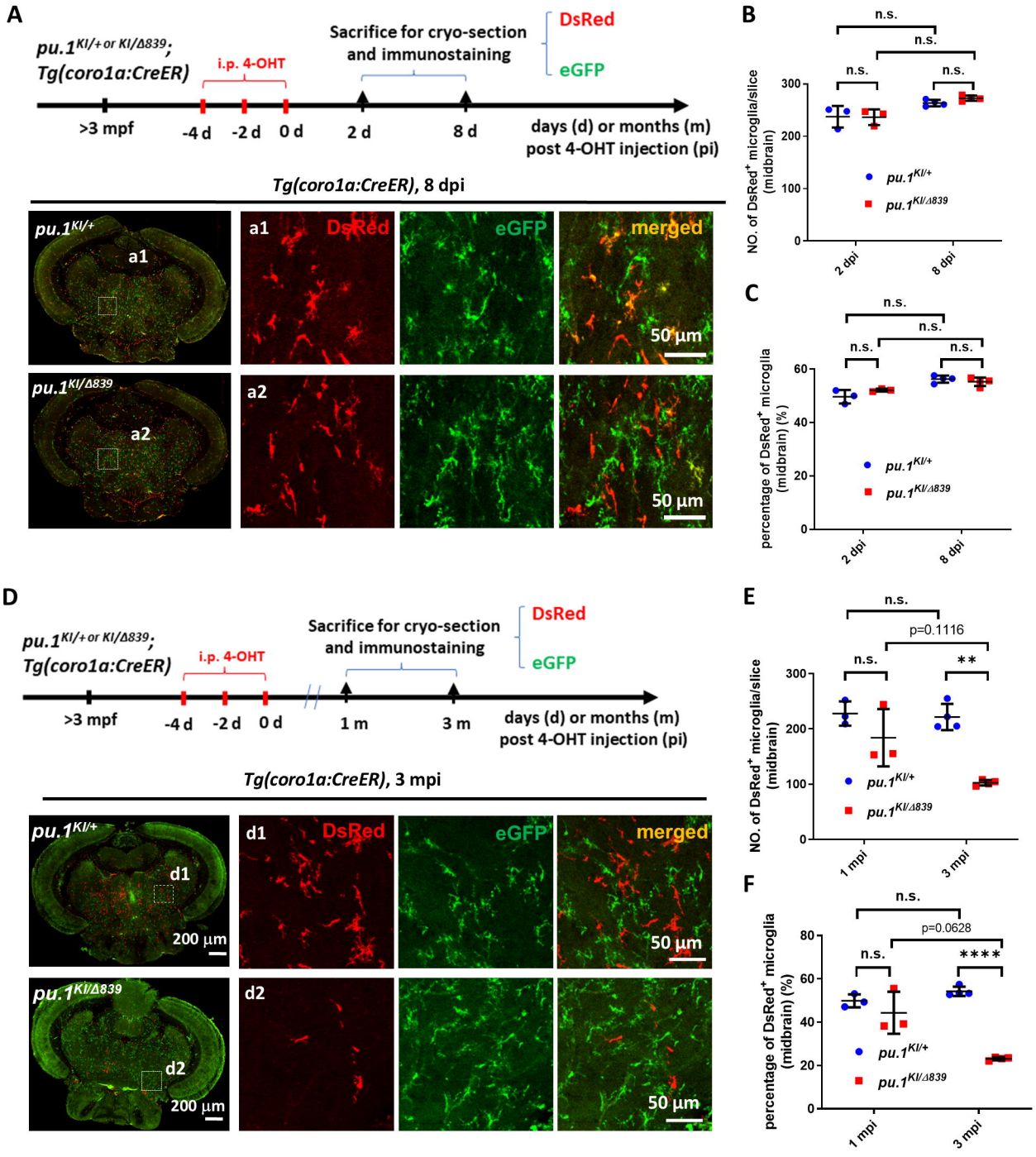
A
pu.1KI/+ or KI/Δ839;
Tg(coro1a:CreER)
i.p. 4-OHT
Sacrifice for cryo-section
and immunostaining
DsRed
eGFP
>3 mpf
-4 d
-2 d
0 d
2 d
8 d
days (d) or months (m)
post 4-OHT injection (pi)
Tg(coro1a:CreER), 8 dpi
pu.1KI/+
a1
DsRed
eGFP
merged
50 µm
pu.1KI/Δ839
a2
B
n.s.
NO. of DsRed+ microglia/slice
(midbrain)
pu.1KI/+
pu.1KI/Δ839
2 dpi
8 dpi
C
percentage of DsRed+ microglia
(midbrain) (%)
D
pu.1KI/+ or KI/Δ839;
Tg(coro1a:CreER)
1 m
3 m
Tg(coro1a:CreER), 3 mpi
d1
d2
200 µm
E
p=0.1116
**
1 mpi
3 mpi
F
p=0.0628
****

Figure 4

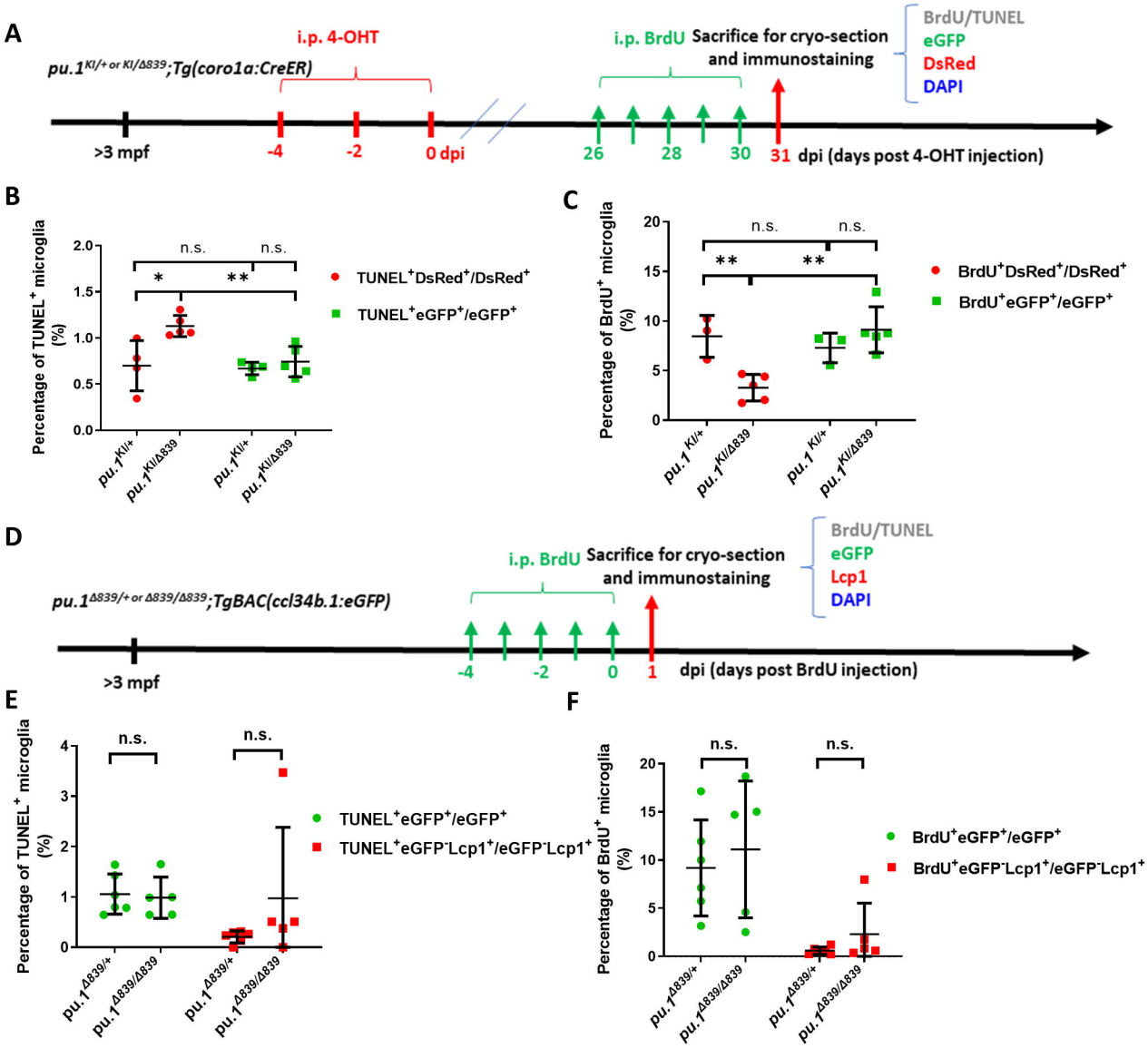
A
pu.1KI/+ or KI/Δ839;Tg(coro1a:CreER)
i.p. 4-OHT
i.p. BrdU
Sacrifice for cryo-section and immunostaining
BrdU/TUNEL
eGFP
DsRed
DAPI
>3 mpf
-4
-2
0 dpi
26
28
30
31 dpi (days post 4-OHT injection)
B
Percentage of TUNEL+ microglia (%)
n.s.
n.s.
*
**
TUNEL+DsRed+/DsRed+
TUNEL+eGFP+/eGFP+
pu.1KI/+
pu.1KI/Δ839
pu.1KI/+
pu.1KI/Δ839
C
Percentage of BrdU+ microglia (%)
n.s.
n.s.
**
**
BrdU+DsRed+/DsRed+
BrdU+eGFP+/eGFP+
pu.1 KI/+
pu.1 KI/Δ839
pu.1 KI/+
pu.1KI/Δ839
D
pu.1Δ839/+ or Δ839/Δ839;TgBAC(ccl34b.1:eGFP)
i.p. BrdU
Sacrifice for cryo-section and immunostaining
BrdU/TUNEL
eGFP
Lcp1
DAPI
>3 mpf
-4
-2
0
1
dpi (days post BrdU injection)
E
Percentage of TUNEL+ microglia (%)
n.s.
n.s.
TUNEL+eGFP+/eGFP+
TUNEL+eGFP-Lcp1+/eGFP-Lcp1+
pu.1Δ839/+
pu.1Δ839/Δ839
pu.1Δ839/+
pu.1Δ839/Δ839
F
Percentage of BrdU+ microglia (%)
n.s.
n.s.
BrdU+eGFP+/eGFP+
BrdU+eGFP-Lcp1+/eGFP-Lcp1+
pu.1Δ839/+
pu.1Δ839/Δ839
pu.1Δ839/+
pu.1Δ839/Δ839

Figure 5

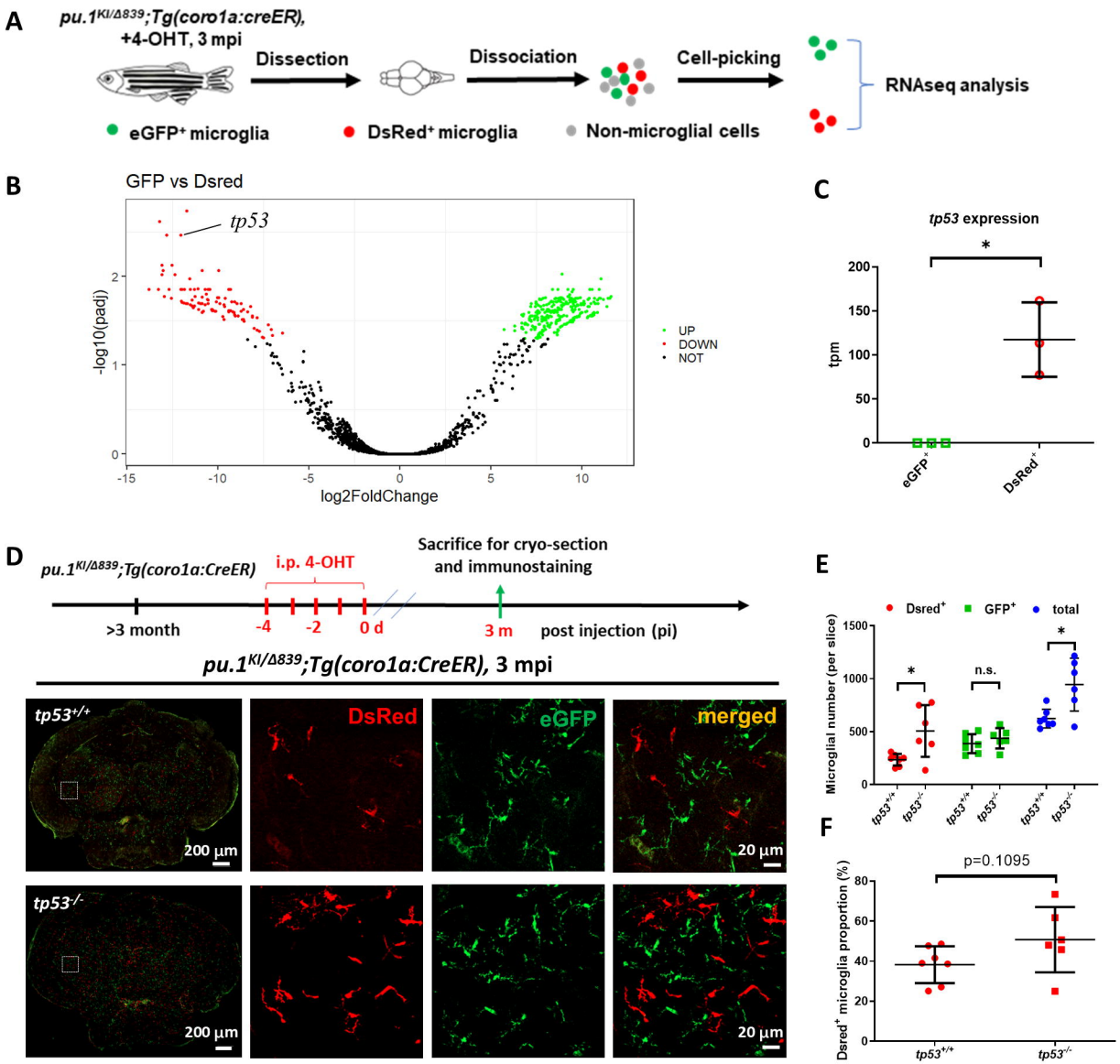
A
pu.1KI/Δ839;Tg(coro1a:creER),
+4-OHT, 3 mpi
Dissection
Dissociation
Cell-picking
RNAseq analysis
eGFP+ microglia
DsRed+ microglia
Non-microglial cells
B
GFP vs Dsred
tp53
-log10(padj)
log2FoldChange
UP
DOWN
NOT
C
tp53 expression
tpm
eGFP+
DsRed+
D
pu.1KI/Δ839;Tg(coro1a:CreER)
i.p. 4-OHT
Sacrifice for cryo-section
and immunostaining
>3 month
-4
-2
0 d
3 m
post injection (pi)
pu.1KI/Δ839;Tg(coro1a:CreER), 3 mpi
tp53+/+
tp53-/-
DsRed
eGFP
merged
200 µm
20 µm
E
Dsred+
GFP+
total
Microglial number (per slice)
n.s.
F
p=0.1095
Dsred+ microglia proportion (%)

Figure 6

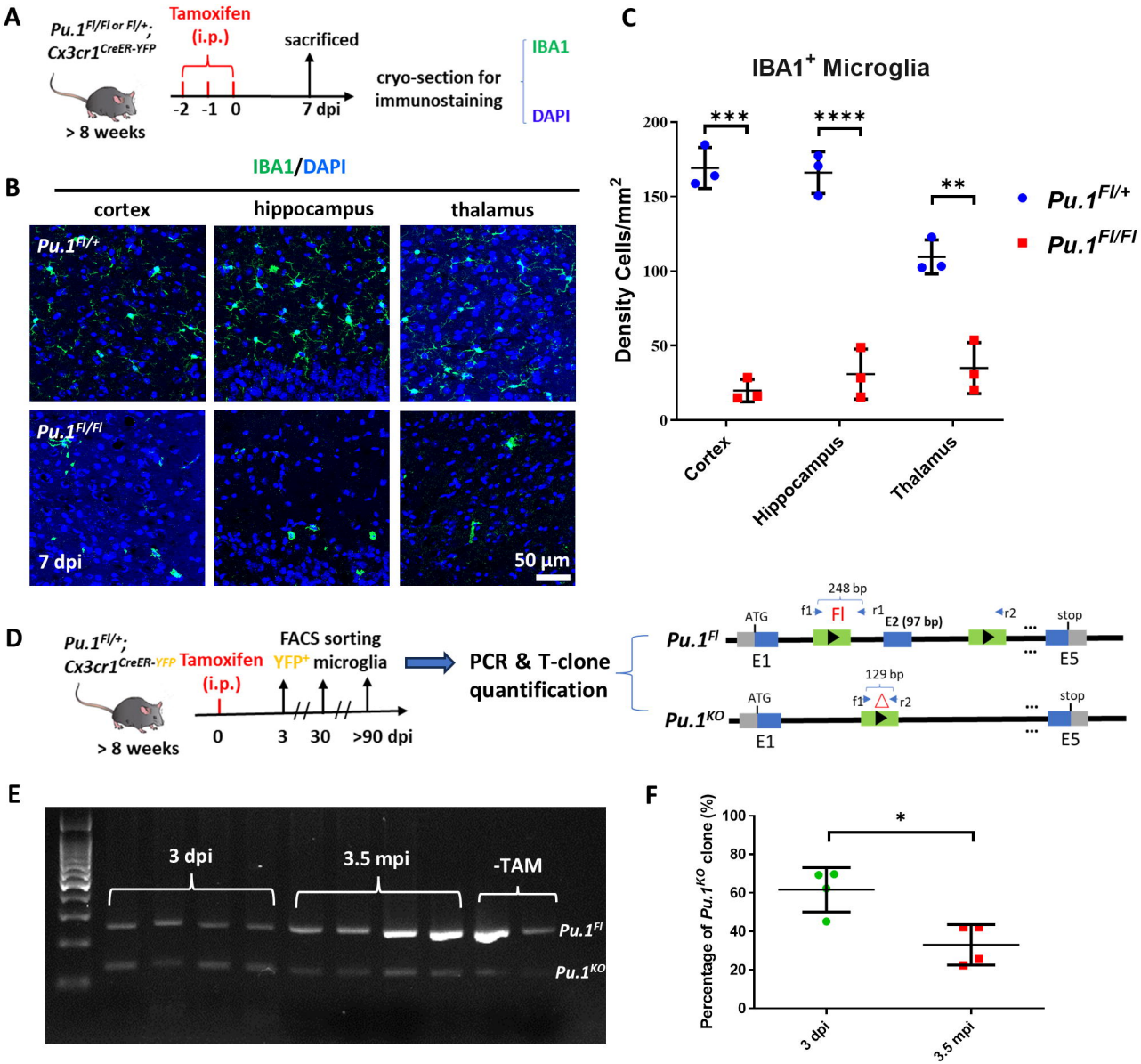
A
Pu.1Fl/Fl or Fl/+; Cx3cr1CreER-YFP
> 8 weeks
Tamoxifen (i.p.)
-2 -1 0
7 dpi
sacrificed
cryo-section for immunostaining
IBA1
DAPI
B
IBA1/DAPI
cortex
hippocampus
thalamus
Pu.1Fl/+
Pu.1Fl/Fl
7 dpi
50 µm
C
IBA1+ Microglia
Density Cells/mm2
200
150
100
50
0
***
****
**
Pu.1Fl/+
Pu.1Fl/Fl
Cortex
Hippocampus
Thalamus
D
Pu.1Fl/+; Cx3cr1CreER-YFP
> 8 weeks
Tamoxifen (i.p.)
FACS sorting YFP+ microglia
0
3
30
>90 dpi
PCR & T-clone quantification
248 bp
f1
Fl
r1
E2 (97 bp)
r2
ATG
stop
Pu.1Fl
E1
E5
129 bp
Pu.1KO
E
3 dpi
3.5 mpi
-TAM
Pu.1Fl
Pu.1KO
F
Percentage of Pu.1KO clone (%)
100
80
60
40
20
0
*
3 dpi
3.5 mpi